NEURORADIOLOGICAL FINDINGS WITH CONVENTIONAL AND ADVANCED MRI TECHNIQUES IN SECONDARY HEADACHES

Danai-Eleni Stefanou[1], Maria-Ioanna Stefanou[2], Vasileios K. Katsaros[1, 3-5]

[1] Department of Advanced Imaging Modalities, MRI Unit, General Anticancer and Oncological Hospital of Athens "St. Savvas", Athens
[2] 2nd Department of Neurology, National and Kapodistrian University of Athens, "Attikon" University Hospital, Athens
[3] 1st Department of Neurosurgery, National and Kapodistrian University of Athens, Evangelismos Hospital, Athens
[4] 1st Department of Neurology, National and Kapodistrian University of Athens, Eginition Hospital, Athens
[5] Department of Neuroradiology, University College London (UCL), London

Abstract

Headache is one of the most common clinical entities that neurologists are confronted with in clinical practice and is associated with a wide spectrum of differential diagnoses. The International Classification of Headache Disorders, 3rd edition (ICHD-III) classifies headache in two main categories: primary headache in the absence of underlying disorder and secondary headache which is attributed to underlying systemic or neurological disease. The classification of headache warrants a detailed patient history and clinical examination, as well as complementary neuroradiological studies, especially when "red flags" point towards secondary headache types that may require therapeutic interventions. The main causes of secondary headache include infections, neuroinflammatory disorders, brain neoplasms, cerebrovascular diseases, and alterations of cerebrospinal fluid (CSF) dynamics. Computed Tomography (CT) studies are primarily used for the acute differential diagnosis of headache, for example in patients presenting with "thunderclap-headache" when subarachnoid haemorrhage is suspected. In the sub-acute setting, however, Magnetic Resonance imaging (MRI) studies are far more sensitive for the delineation of underlying brain pathologies. Besides the use of conventional MRI, advanced MRI techniques, including diffusion imaging, perfusion, spectroscopy and functional MRI, facilitate the early diagnosis of underlying functional, structural, and metabolic changes, while they may be also utilized for treatment monitoring in patients with secondary headaches. In the present review, the most commonly encountered secondary headaches along with associated neuroradiological findings will be presented, focusing on conventional and advanced MRI techniques.

Key words: Magnetic Resonance Imaging (MRI), secondary headache, advanced MRI techniques, neuroradiology

ΝΕΥΡΟΑΚΤΙΝΟΛΟΓΙΚΑ ΕΥΡΗΜΑΤΑ ΜΕ ΣΥΜΒΑΤΙΚΕΣ ΚΑΙ ΠΡΟΗΓΜΕΝΕΣ ΤΕΧΝΙΚΕΣ ΑΠΕΙΚΟΝΙΣΗΣ ΜΑΓΝΗΤΙΚΟΥ ΣΥΝΤΟΝΙΣΜΟΥ ΣΤΙΣ ΔΕΥΤΕΡΟΠΑΘΕΙΣ ΚΕΦΑΛΑΛΓΙΕΣ

Δανάη-Ελένη Στεφάνου[1], Μαρία-Ιωάννα Στεφάνου[2], Βασίλειος Κ. Κατσαρός[1, 3-5]

[1] Τμήμα Νεότερων Απεικονιστικών Μεθόδων, Μονάδα Απεικόνισης Μαγνητικού Συντονισμού, Γενικό Αντικαρκινικό και Ογκολογικό Νοσοκομείο Αθηνών, «Ο Άγιος Σάββας», Αθήνα
[2] Β΄ Νευρολογική Κλινική Ιατρικής Σχολής, Εθνικό και Καποδιστριακό Πανεπιστήμιο Αθηνών, Νοσοκομείο «Αττικόν», Αθήνα
[3] Α΄ Νευροχειρουργική Κλινική Ιατρικής Σχολής, Εθνικό και Καποδιστριακό Πανεπιστήμιο Αθηνών, Νοσοκομείο Ευαγγελισμός, Αθήνα
[4] Α΄ Νευρολογική Κλινική Ιατρικής Σχολής, Εθνικό και Καποδιστριακό Πανεπιστήμιο Αθηνών, Νοσοκομείο Αιγινήτειο, Αθήνα
[5] Τμήμα Νευροακτινολογίας, University College London (UCL), London

Περίληψη

Η κεφαλαλγία είναι ένα από τα συχνότερα συμπτώματα που καλούνται να αξιολογήσουν οι νευρολόγοι στην κλινική πράξη και σχετίζεται με ένα ευρύ φάσμα διαφορικής διάγνωσης. Η Διεθνής Ταξινόμηση Διατα-

ραχών Κεφαλαλγίας, 3η έκδοση (ICHD-III) ταξινομεί την κεφαλαλγία σε δύο κύριες κατηγορίες: πρωτοπαθή κεφαλαλγία απουσία υποκείμενης διαταραχής και δευτεροπαθή κεφαλαλγία που αποδίδεται σε υποκείμενη συστηματική ή νευρολογική νόσο. Η ταξινόμηση της κεφαλαλγίας απαιτεί λήψη λεπτομερούς ιστορικού και ενδελεχή κλινική εξέταση του ασθενούς, καθώς και συμπληρωματική νευροακτινολογική μελέτη, ειδικά όταν συνυπάρχουν ευρήματα που υποδεικνύουν την παρουσία υποκείμενης νόσου που πιθανώς απαιτεί άμεση θεραπευτική παρέμβαση. Οι κύριες αιτίες της δευτεροπαθούς κεφαλαλγίας περιλαμβάνουν λοιμώξεις, φλεγμονώδεις διαταραχές του κεντρικού νευρικού συστήματος, νεοπλάσματα του εγκεφάλου, αγγειακές παθήσεις και μεταβολές της δυναμικής της ροής του εγκεφαλονωτιαίου υγρού (ΕΝΥ). Η διενέργεια υπολογιστικής τομογραφίας (CT) πραγματοποιείται κυρίως σε οξεία φάση, για τη διαφορική διάγνωση της κεφαλαλγίας, επί παραδείγματι σε ασθενείς που εμφανίζουν «κεραυνοβόλο-κεφαλαλγία» και στους οποίους τίθεται η υπόνοια υπαραχνοειδούς αιμορραγίας. Ωστόσο, στην υποξεία φάση, η Απεικόνιση Μαγνητικού Συντονισμού (MRI) έχει μεγαλύτερη ευαισθησία στην αναγνώριση και λεπτομερή αξιολόγηση υποκείμενων αλλοιώσεων του εγκεφάλου. Η συνδυαστική εφαρμογή των συμβατικών τεχνικών Απεικόνισης Μαγνητικού Συντονισμού και των προηγμένων τεχνικών νευροαπεικόνισης, συμπεριλαμβανομένης της απεικόνισης τανυστή διάχυσης, της αιματικής διήθησης πρώτης διόδου, της φασματοσκοπίας και της λειτουργικής Απεικόνισης Μαγνητικού Συντονισμού, διευκολύνει την έγκαιρη διάγνωση και αξιολόγηση μορφολογικών, λειτουργικών και μεταβολικών αλλαγών, όπως επίσης και την παρακολούθηση της θεραπείας ασθενών με δευτεροπαθή κεφαλαλγία. Στην παρούσα ανασκόπηση θα παρουσιαστούν τα συχνότερα αίτια δευτεροπαθούς κεφαλαλγίας και τα νευροακτινολογικά τους ευρήματα, εστιάζοντας κυρίως στις συμβατικές και προηγμένες τεχνικές MRI.

Λέξεις ευρετηρίου: Απεικόνιση Μαγνητικού Συντονισμού (MRI) εγκεφάλου, δευτεροπαθής κεφαλαλγία, προηγμένες τεχνικές απεικόνισης Μαγνητικού Συντονισμού, Νευροακτινολογία

Introduction

Headache is one of the most common symptoms that a patient will experience during his lifetime and one of the most frequent disabling diseases worldwide [1]. According to the International Classification of Headache Disorders (ICHD-III) [2], headache can be classified in primary and secondary headache, with the latter being attributed to underlying causal factors, including infections, neuroinflammatory disorders, brain neoplasms, cerebrovascular diseases, and alterations of cerebrospinal fluid (CSF) dynamics (Figure 1). The differential diagnosis between primary and secondary headache warrants thorough neurological examination, as well as the acquisition of a detailed patient history. If the findings of the clinical examination and patient history are not consistent with primary headache, then secondary headache types are assumed. In such cases, further investigations, including neuroradiological studies are indicated. In clinical practice, a useful mnemonic for the identification of "red flags" that should prompt physicians to indicate neuroimaging studies is SNOOP4 (S: systemic symptoms/signs, N: abnormal findings on neurological examination, O: sudden onset, O: older age at onset above 50 years, P4: positional headache, precipitated by Valsalva maneuver or exercise, progressive headache, papilledema) (Table 1) [3].

The National Institute for Health and Care Excellence (NICE) and the American Headache Society (AHS) guidelines do not recommend neuroimaging studies for patients with normal neurological examination, stable headache without atypical features, that fulfil the diagnostic criteria for a primary headache, while – with the exception of subarachnoid

Figure 1. Secondary Headache Disorder Aetiology according to the International Classification of Headache disorders, 3rd edition, beta version

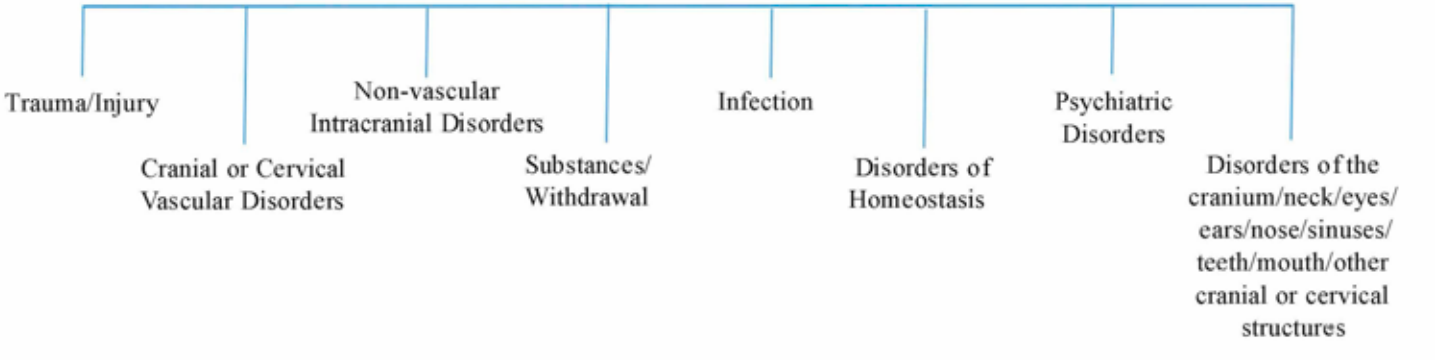

Table 1. Red flag signs for the diagnosis of headaches (SNOOP4)

Mnemonic	Presentation
Systemic symptoms	• Fever of unidentified cause, weight loss, chills and myalgia • Malignancy, immunocompromised patient
Neurological symptoms	• Signs of motor weakness and sensory loss, diplopia or ataxia • Abnormal signs in neurological examination
Onset sudden	• Thunderclap headache, sudden onset, with peak intensity in <1 minute
Onset after age 50 years	• Onset after the age of 50 years
P 4	• Progressive headache or pattern change • Headache worsening after Valsalva manoeuvre • Postural aggravation • Papilledema

hemorrhage and in emergency settings – Computed Tomography (CT) should not be performed if Magnetic Resonance Imaging (MRI) is available [4-7]. Conversely, neuroimaging should be performed in all patients presenting with atypical symptoms and signs, for example irregular or new headache patterns; increase in the severity of headache; history of epileptic seizures or head trauma; history of malignancy, active infections, stroke or intracranial bleeding; focal or new neurological deficits; and other "red flags" that may be suggestive of an underlying disorder [5, 8, 9].

Besides the choice of imaging modality (CT versus MRI), the diagnostic protocols also depend on several factors, including patient history, headache pattern, duration, intensity and presence of concomitant neurological signs, as well as depending on whether new-onset or recurrent headache is being investigated [9, 10]. Overall, MRI has a superior sensitivity compared to CT, especially for depicting abnormalities in the posterior fossa, acute ischemic lesions, and mass lesions, while simultaneous performance of an expanded MRI protocol with advanced MRI methods may enable accurate differential diagnosis and treatment planning [11]. It should be noted that the differential diagnosis of headache is practically exhaustive, since headache can comprise an epiphenomenon of many neurological or systemic diseases [1, 2].

Herein, we will review the most commonly encountered causal factors of secondary headache along with the associated neuroradiological findings, focusing on conventional and advanced MRI techniques.

Secondary headache attributed to cranial or cervical vascular disorder

Craniocervical artery dissection

Craniocervical artery dissection (CAD) is a frequent cause of ischemic stroke in young and middle-aged adults [12]. Prompt and accurate CAD diagnosis is essential for the identification of the underlying stroke aetiology and prevention of stroke recurrence [13, 14]. The clinical presentation of CAD is variable, ranging from mild symptoms, including neck pain, Horner's syndrome and headache, to severe stroke syndromes [14, 15]. Notably, the headache in CAD is typically ipsilateral to the dissection site [13]. In affected patients, ultrasonography may provide direct or indirect evidence indicative of CAD [16]; in the majority of cases, however, neuroimaging studies including Computed tomography angiography (CTA), MR angiography (MRA), or Digital subtraction angiography (DSA) are required to establish CAD diagnosis.

With respect to CT neuroimaging studies, CTA can provide images of high-resolution and contrast for depiction of the arterial lumen and wall. Two-dimensional (2D) and three-dimensional (3D) reconstruction methods can be employed to construct images comparable to those acquired by DSA, although DSA is still considered the gold standard method for CAD diagnosis [17]. The most typical imaging finding of CAD on CT imaging, with high specificity but low sensitivity, is the so-called "target sign", which is characterized by a narrowed eccentric lumen surrounded by a hyperdense crescent-shaped mural thickening and thin peripheral enhancement [18]. Additional imaging findings suggestive of CAD include the depiction of an intimal flap and a dissecting aneurysm [18].

With respect to MR imaging studies, MRI and MRA have been shown to have an excellent sensitivity of approximately 87-99%, compared with DSA for the diagnosis of internal carotid artery (ICA) dissection. However, the sensitivity of MRA is reduced to 60% for vertebral artery (VA) dissection due to the low calibre of VA and a flow-related enhancement of the paravertebral veins that may be misinterpreted as CAD [19]. Consequently, if VA dissection is suspected,

Figure 2. On axial T2W image (A), a dilated left vertebral artery is depicted along with an hyperintense linear intimal flap. (B) On contrast-enhanced 3D black blood T1W the wall of the left vertebral artery, as well as the intimal flap showed marked enhancement, imaging findings suggesting left vertebral artery dissection. (Reprinted with permission from Wang, YM. *et al.* Chinese specialist consensus on imaging diagnosis of intracranial arterial dissection. *Chin Neurosurg Jl* **3**, 30 (2017). https://doi.org/10.1186/s41016-017-0095-2)

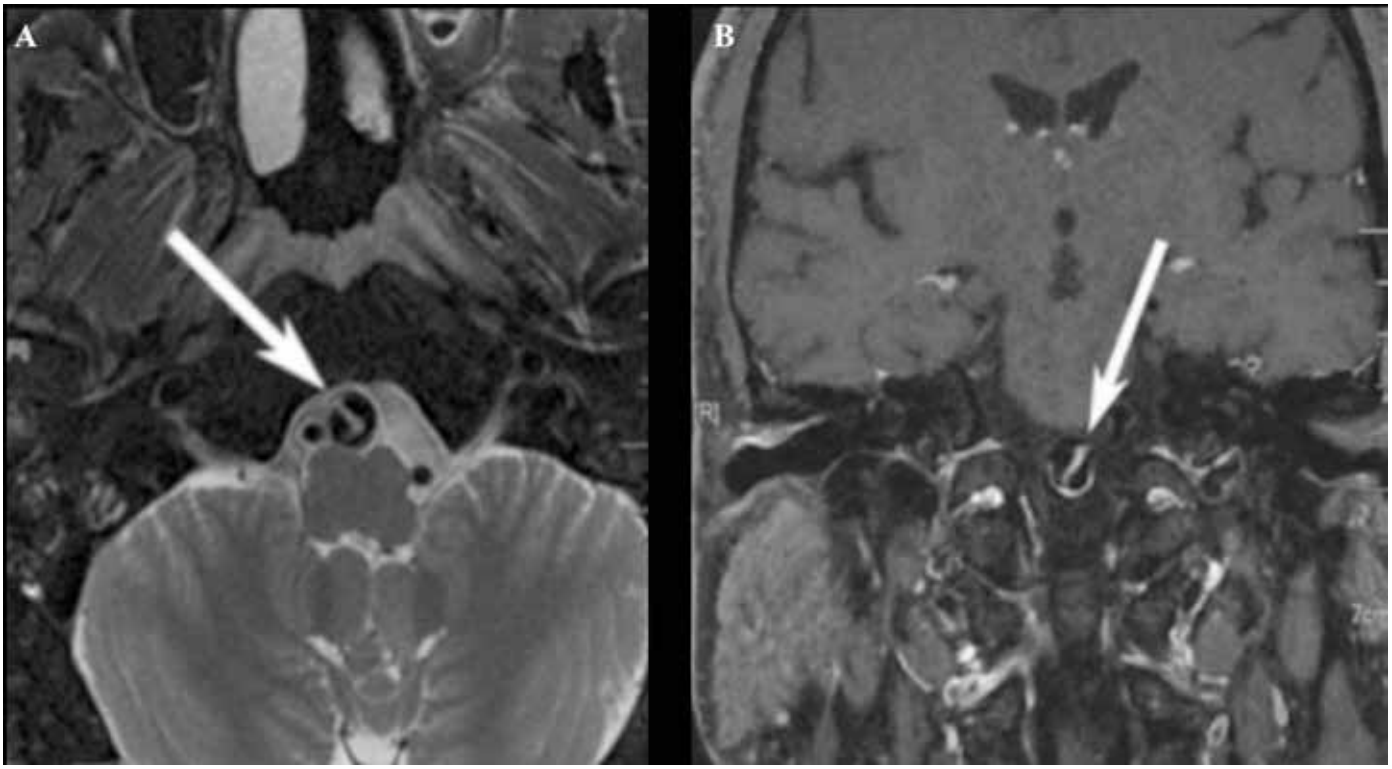

CTA should be performed due to its higher diagnostic sensitivity compared to MRA [19-21]. Notably, contrast-enhanced MRA may provide better results compared to 3D time-of-flight (TOF) MRA [19]. A crescent-shaped intramural hematoma is the most common finding of ICA and VA dissection on MRI. The signal intensity of the hematoma is analogous to the products of haemoglobin breakdown and their paramagnetic effects. In the acute phase, the intramural hematoma may be obscured on T1W fat-saturated images, while in the subacute phase (7 days to 2 weeks post-dissection) the hematoma is depicted with high signal [21]. Additional MRI findings of CAD include narrowed eccentric lumen and increased external diameter of the artery. More recently, heavily T1-weighted flow-suppressed sequences, such as magnetization-prepared rapid acquisition gradient–recalled echo (MPRAGE), have also been implemented to detect carotid intraplaque haemorrhage in CAD [22]. Moreover, 3D black-blood fat-saturated T1W sequence has been shown to have high sensitivity for the depiction of intramural hematoma [23]. Additionally, vessel wall imaging sequences may be performed in addition to TOF-MRA, in order to assess the luminal calibre. Finally, a 3D simultaneous non-contrast angiography and intraplaque haemorrhage (SNAP) MRI technique has been recently introduced to provide information both regarding the arterial wall and the arterial lumen in a single scan [23, 24] (Figure 2).

Vasculitis

Headache may be the only presenting symptom of giant cell arteritis (GCA), and GCA should always be considered in elderly patients (especially women) presenting with new-onset headache [25]. GCA –also known as temporal arteritis– is a granulomatous vasculitis mainly affecting medium and large sized arteries. The main histological feature of GCA is granulomatous arterial inflammation caused by lymphocytes, histiocytes, and multinucleated giant cells [26]. It must be mentioned that in GCA, unaffected areas may be noted between the inflamed arterial sites, which are known as "skip lesions". Biopsy results are false-negative in approximately 8-28% of GCA patients, especially when biopsy is taken from normal-appearing lesions, i.e., not guided by imaging studies [27]. Although temporal artery biopsy comprises the gold standard for GCA diagnosis, neuroimaging studies are increasingly used in clinical practice for GCA diagnosis, for biopsy plan-

Figure 3. (A) On axial FLAIR image, a high-intensity lesion in the white matter on the left temporal lobe is depicted, which is a non-specific finding. (B) MR angiography shows multifocal segmental narrowing of right and left middle cerebral artery and left anterior cerebral artery(arrows), suggesting primary angiitis of the CNS (PACNS)

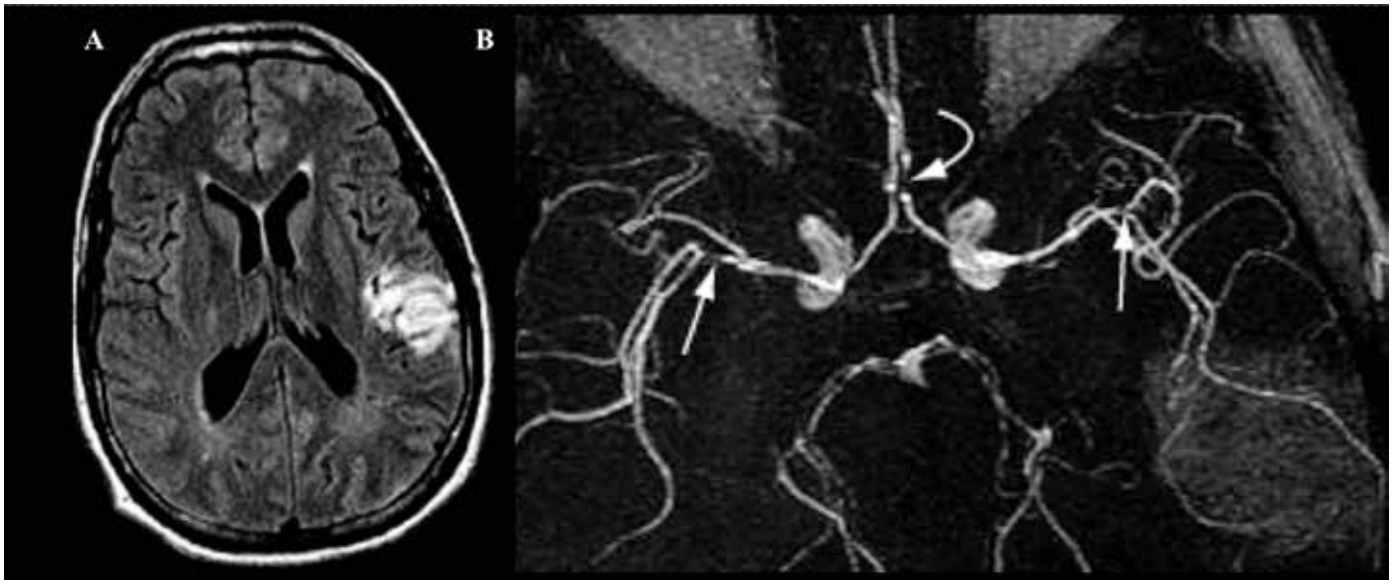

ning, as well as for treatment monitoring [28]. Advanced MRI sequences, such as the 3D black-blood fat-saturated T1W sequence, facilitate the depiction of mural inflammation and allow measurement of the mural thickening and quantification of the contrast enhancement [29]. Furthermore, TOF MRA can depict the luminal diameter, which appears decreased in regions affected by GCA [30]. The combination of the two aforementioned MRI techniques has been shown to have a high sensitivity and specificity for GCA diagnosis, of 80% and 100% respectively compared to the gold standard of temporal artery biopsy [30].

Headache, when accompanied by encephalopathy, may also be a presenting symptom of primary angiitis of the central nervous system (PACNS). Although PACNS is a rare nosological entity, high clinical awareness is warranted in patients presenting with headache and encephalopathy, and atypical ischemic strokes. Ischemic infarctions are noted on neuroimaging in approximately 53% of PACNS cases [31]. Conventional MRI techniques reveal multiple infarctions, which are typically bilaterally located, in various stages of healing, of variable size and affecting different vascular territories [32]. Vessel wall MRI (VW-MRI) can also be applied for the diagnosis of PACNS, depicting prominent vessel wall enhancement [33]. Notably, PACNS should be differentiated from vasculitis that may be secondary to other causes, including infection, systemic disease, malignancy, drug use, or radiation therapy, and histological confirmation is required for definite PACNS diagnosis [32, 34] (Figure 3).

Cerebral venous sinus thrombosis (CVST)

Headache, focal neurological deficits, epileptic seizures, intracranial hypertension and encephalopathy comprise frequent clinical presentations of CVST, with varying intensity depending on the site of venous thrombosis [35]. Headache is present in more than 85% of CVST patients [36, 37]. Although CVST-associated headache may be accompanied by nausea, vomiting, papilledema, and visual disturbances, in some cases headache may be the only CVST presenting symptom. The spectrum of headache patterns associated with CVST is very wide, but the most commonly encountered is subacute-onset headache with rapid worsening, that may mimic subarachnoid haemorrhage, migraine or intracranial hypertension [38, 39].

Neuroimaging studies comprise the cornerstone of CVST diagnosis and aim to answer: (1) whether there is evidence of cerebral venous occlusion; (2) whether there are findings of parenchymal or other intracranial lesions; (3) which is the underlying cause of CVST [40, 41]. In more than 85% cases of CVST cases, a prothrombotic risk factor or a direct underlying cause can be identified, while multiple CVST causes can be found in approximately 1/3 of cases [35]. Furthermore, neuroimaging studies are additionally used for the follow-up of CVST patients, depicting the venous recanalization and treatment response, and for excluding CVST complications or recurrence.

CT is considered as first-line imaging modality for patients admitted to the emergency room (ER) with suspected CVST. Non-enhanced brain CT may depict

Figure 4. A 65-year-old male presented with headache. (A) Time-of-flight (TOF) MR venography shows absence of normal flow signal in the left transverse and left sigmoid sinuses, indicating CVST. (B) Axial contrast-enhanced MRV depicts a filling defect in the left transverse sinus, corresponding to a nonenhanced ovoid thrombus

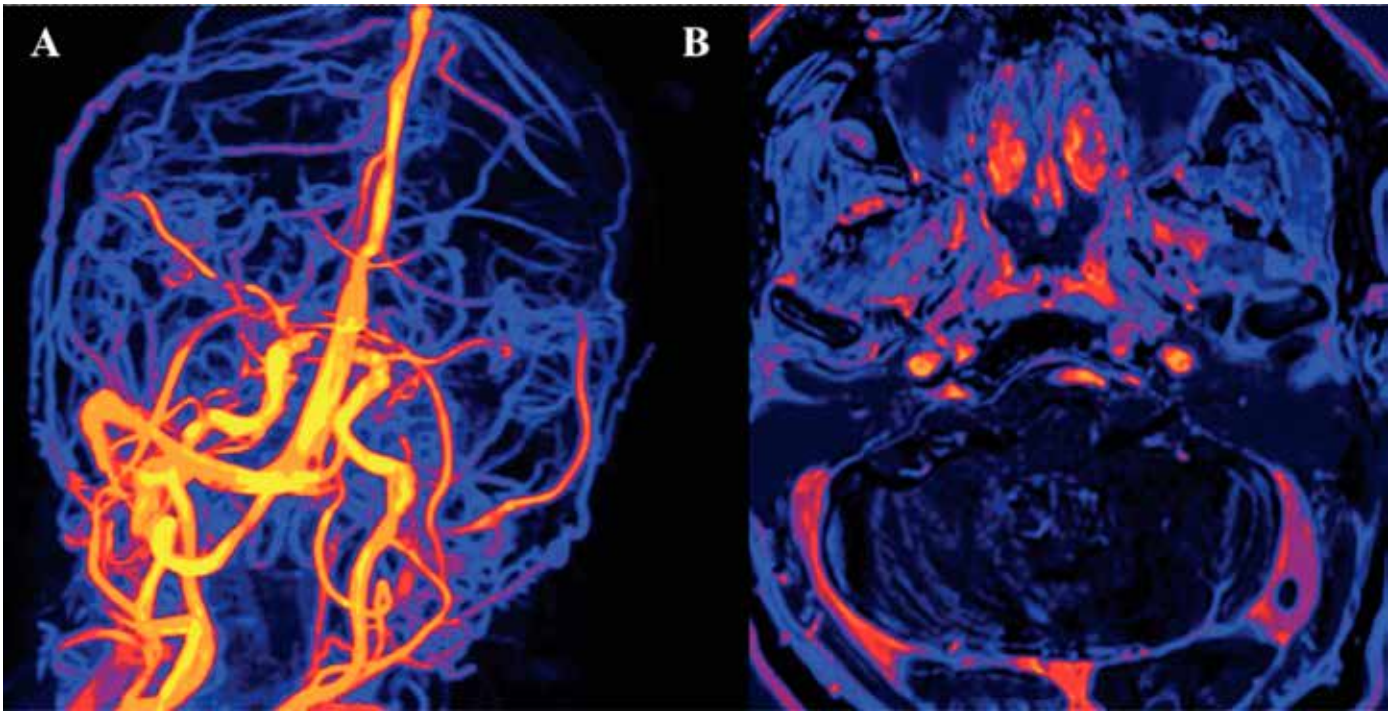

hyperdense thrombus in the dural sinus ("dense triangle sign") or in cortical veins ("cord sign"), but in up to 2/3 of CVST cases the findings of non-contrast-enhanced brain CT are false negative [42]. By contrast, CT venography (CTV) has a 95% sensitivity for CVST diagnosis compared to DSA as the gold standard [43].

In CVST patients, MRI findings are time dependent, as the signal intensity of the thrombus may vary according to the haemoglobin degradation [44]. Phase-contrast and time of flight MRV may detect CVST, but each technique has limitations and disadvantages (Figure 4). Contrast-enhanced MR-venography (MRV) is highly accurate in diagnosing CVST at all stages, including the chronic stage compared to any other type of MRV [45]. Digital subtraction angiography (DSA), albeit considered the gold standard for CVST diagnosis, is nowadays reserved for patients that may require endovascular treatment [46].

Parenchymal abnormalities as consequence of CVST include venous infraction, intraparenchymal and subarachnoid haemorrhage, hydrocephalus due to impaired CSF absorption and brain edema are better assessed on MRI rather than on CT [47]. Use of Diffusion weighted imaging (DWI) and apparent diffusion coefficient (ADC) map can facilitate the distinction between vasogenic and cytotoxic brain edema, that may coexist in CVST [48, 49]. Finally, it should be stressed that neuroimaging is important for exclusion of CVST recurrence which affects approximately 12-13% of patients [50].

Subarachnoid Haemorrhage (SAH)

Thunderclap headache is a characteristic manifestation of subarachnoid haemorrhage (SAH). Typically, patients describe this type of headache as the "worst headache of their life" [37]. SAH is classified in traumatic and spontaneous SAH. Among the causes of spontaneous SAH, rupture of intracranial aneurysms accounts for up to 85% of SAH cases [51]. The remaining 15% of SAH patients have no discernible cause of bleeding [52]. Crucially, perimesencephalic SAH is a distinct type of SAH, that accounts for 5% of all SAH cases and is related to underlying venous drainage anomalies rather than underlying aneurysms [53].

On neuroimaging, the distribution and epicentre of SAH can indicate the localization of a ruptured aneurysm or other underlying pathologies that may precipitate non-aneurysmal SAH. For example, the presence of convexity SAH sparing the basal cisterns, the Sylvian fissure, the interhemispheric fissure or the ventricles with additional imaging findings of microbleeds and cortical superficial siderosis may indicate cerebral amyloid angiopathy as the underlying cause of SAH [54]. With respect to aneurysmal SAH, the most frequent localization of aneurysms in approximately 90% of cases involves the anterior circulation [55].

Figure 5. Post traumatic subarachnoid haemorrhage (SAH). Acute subdural hematoma and acute epidural hematoma is depicted on the right hemisphere and along the tentorium cerebelli. Additionally, hyperdense material is seen filling the sulci adjacent to the subdural and epidural hematoma, suggestive of traumatic SAH. Secondary features of mass effects are depicted, including midline shift and right ventricle compression

With respect to CT studies, (Figure 5), in a patient presenting with thunderclap headache it is pivotal to indicate emergent CT scan, that besides native CT should include CTA for exclusion of underlying aneurysms. For the detection of aneurysms >3 mm, CTA –especially using subtraction and three-dimensional reconstructions– has a sensitivity and specificity that approaches 100% and is thus, comparable to that of DSA [56, 57]. Nonetheless, DSA remains the gold standard for the definitive detection or exclusion of underlying intracranial aneurysms, and is superior to CTA for detection of small-sized aneurysms (Figure 6). Moreover, DSA is indicated for patients that may require endovascular treatment.

With respect to MRI findings of aneurysmal SAH, the fluid-attenuated inversion recovery (FLAIR) MRI sequence is sensitive for depicting SAH in the first 12 hours, when SAH appears as hyperintensity in the subarachnoid spaces. FLAIR is superior to CT for subacute and chronic SAH, as "aging" hematoma is difficult to capture on CT in subacute and chronic stages [58, 59]. MRA has a sensitivity of approximately 80% for depicting cerebral aneurysms, but its sensitivity is lower for detection of small aneurysms (diameter <3mm in maximum diameter) and aneurysms located at the internal carotid artery and anterior cerebral artery [60]. The sensitivity of gradient echo (GRE) sequences differs between the different SAH stages, ranging from a 94% sensitivity during the early SAH stages (up to 4 days), to a 100% sensitivity beyond the acute SAH stage (after 4 days from index event) [61]. Importantly, DWI may demonstrate early ischemic changes associated with SAH or delayed ischemic changes associated with vasospasm, which may complicate up to 20% of SAH cases [62]. MR perfusion can be a useful tool for the diagnosis of cerebral ischemia and evaluation of the cerebral blood flow [63]. Besides the acute SAH diagnosis, it is important to note that MRI has an additional role in excluding concomitant aneurysms, that are not ruptured or may have undergone subclinical rupture (as indicated by haemoglobin products depicted on GRE sequences), as well as for treatment follow-up (i.e., in patients with vasospasms undergoing vasodilator therapy, or patients with aneurysms treated with non-ferromagnetic clips or endovascular therapy).

Reversible Cerebral Vasoconstriction Syndrome (RCVS)

RCVS is clinically characterized by thunderclap headache, which is pathophysiologically related to reversible vasoconstriction of the cerebral arteries. The headache is mainly localized in the occipital lobes, but in some cases may be diffuse. RCVS may be noted in the post-partum period, while typical risk factors include the use of vasoactive substances and drugs (i.e., marijuana, cocaine) [64]. Diagnostic criteria for RCVS have been suggested with 98-100% specificity including: (i) thunderclap headache with periodical recurrence; or (ii) single thunderclap headache either without evident abnormality on neuroimaging or with neuroimaging evidence of watershed infarct/vasogenic edema; or (iii) abnormal angiographic findings with normal neuroimaging and no headache [65]. At symptom onset, neuroimaging may be normal in approximately 50% of RCVS cases [64]. On neuroimaging, RCVS may be diagnosed based on imaging finding either directly pertaining to vascular narrowing or indirectly to RCVS complications (Figure 7).

With respect to CTA, MRA or DSA studies, findings compatible with RCVS include: smooth tapered narrowing from large to medium-sized arteries with concomitant second-order and third-order branch dilatation, which is the so-called "string of beads" appearance of cerebral arteries [66]. Vessel wall MRI (VW-MRI) may be additionally performed in order to exclude arterial wall enhancement, which is typically not present in RCVS, but may be noted in vasculitis and intracranial atherosclerotic plaques [67]. RCVS complications should also be evaluated using CT or

Figure 6. A middle-aged male patient presented with thunderclap headache in the Emergency Room. (A) On axial CT, subarachnoid haemorrhage and intraparenchymal cerebral haemorrhage in the right frontal lobe were noticed. CT angiography did not reveal any aneurysm. (B) On Digital Subtraction Angiography (DSA), a small aneurysm, with diameter less than 3mm, at the right middle cerebral artery was depicted (arrow)

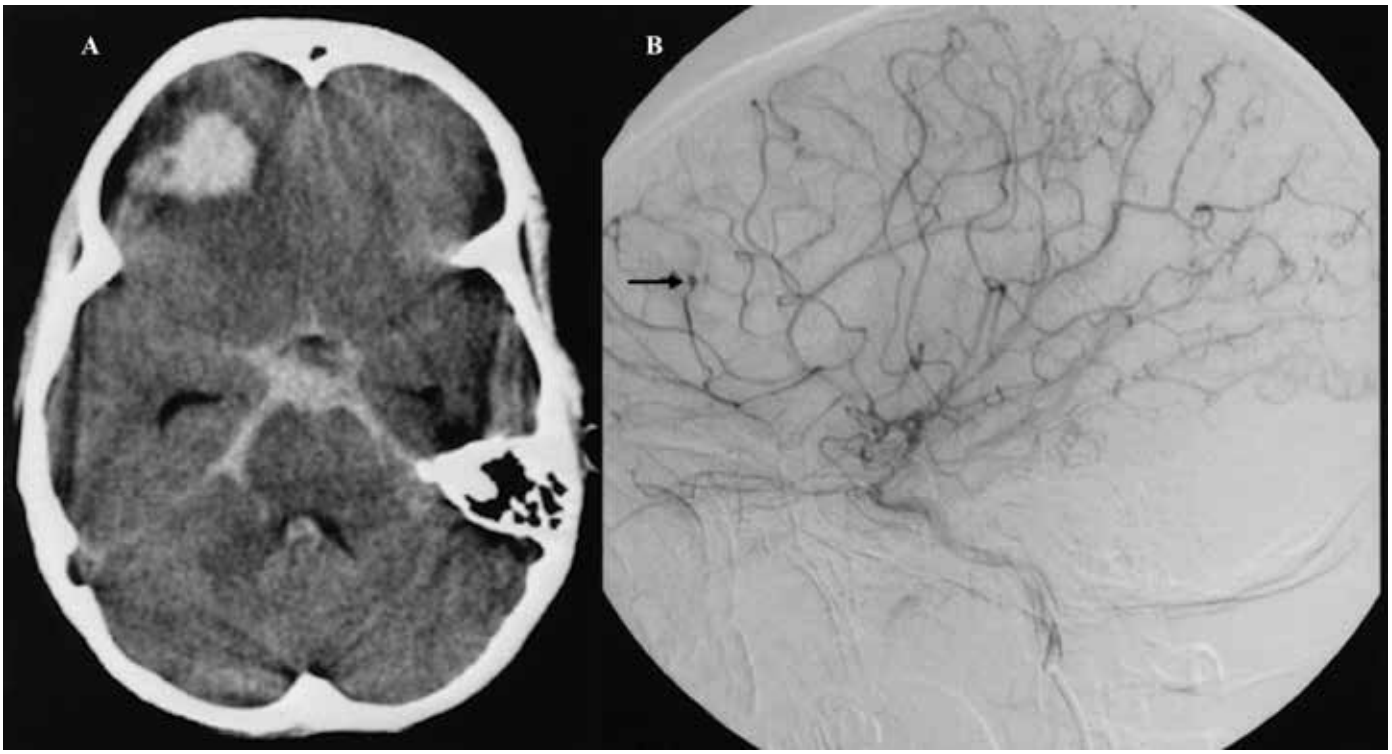

MRI studies, including with decreasing frequency: vasogenic edema (38%), cerebral convexity SAH (22-34%), watershed infarct (29%) or lobar haemorrhage (6-20%) [64, 68]. The typical RCVS course entails resolution of clinical symptoms and neurovascular findings within 8-12 weeks [69].

Cerebral autosomal dominant arteriopathy with subcortical infarcts and leukoencephalopathy (CADASIL)

CADASIL is a rare autosomal dominant microvasculopathy affecting young and middle-aged patients, and is characterized by recurrent subcortical infarcts and leukoencephalopathy, migraine with aura and vascular dementia [70-72]. MRI is the gold standard for CADASIL diagnosis, typically revealing three types of lesions in CADASIL patients: i) widespread confluent white matter hyperintensities, with symmetrical and bilateral tendency, which already at early stages involve the anterior temporal lobe and the external capsule; ii) lacunar infarcts; and iii) cerebral microbleeds [73]. Neuroimaging findings, and particularly the white matter hyperintensities may precede the clinical manifestations of CADASIL (Figure 8). Advanced MR techniques may enable early detection of neuronal loss and demyelination, in regions that may appear normal with conventional MRI techniques. ADC histograms, Diffusion tensor imaging (DTI) and magnetic resonance spectroscopy (MRS) may assess ultrastructural alterations that may be associated with the clinical phenotype [74, 75]. Also, it has been suggested that quantitative diffusion MRI can offer predictive metrics for assessment of CADASIL progression [75, 76].

Secondary headache attributed to non-vascular intracranial disorders

Intracranial Hypotension

Intracranial Hypotension (IH) is a rare syndrome characterised by decreased CSF pressure < 6cm H_2O. A CSF leak along the neuroaxis, in the cervical or thoracic spine in the majority of patients, is the cause of CSF pressure decrease [77, 78]. Typically, IH patients present with a headache with postural pattern, worsening when upright and improving in a recumbent position, with symptom improvement within 15 minutes from lying down. Additional symptoms include vomiting, nausea, vertigo, visual and hearing disturbances and neck pain. According to the causative factor, IH is classified in primary-spontaneous (SIH) and secondary i.e. iatrogenic or traumatic.

Figure 7. A 55-year-old woman who presented with severe headache and developed left-sided weakness. DWI (A) shows multifocal infarcts involving the centrum semiovale and left posterior parietal lobe. On coronal 3D reformatted TOF MRA (B), there is diffuse narrowing of the bilateral middle and anterior cerebral arteries (white arrowheads). Parasagittal postcontrast T1 high-resolution Vessel Wall Imaging (VWI) of the M1 arterial segment of the left MCA (C) shows mild wall thickening and minimal enhancement (similar findings were noted in the right M1 arterial segment, not shown). The patient was diagnosed with RCVS, with subsequent resolution of cerebral vasoconstriction (D)

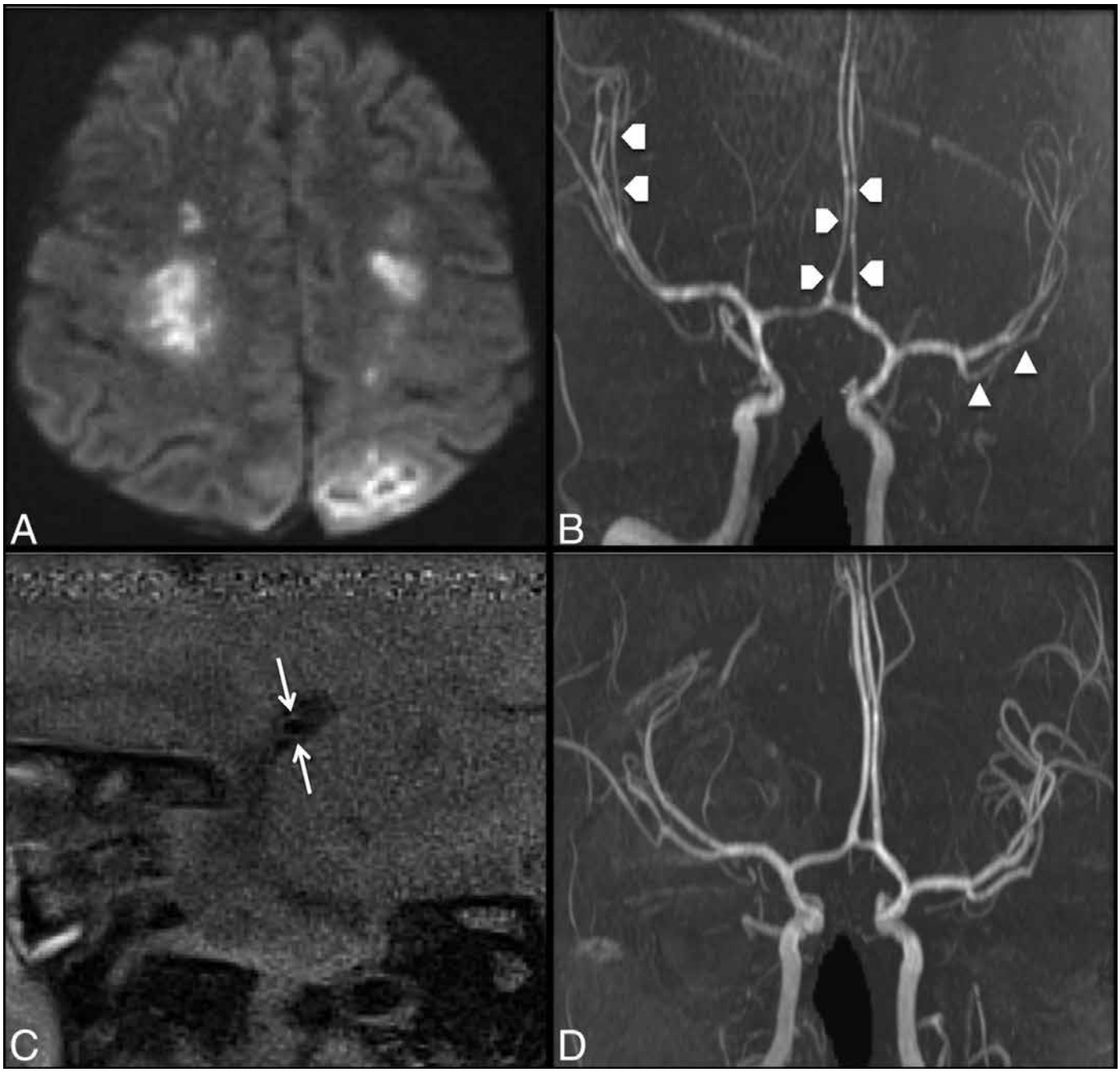

ICHD-3 has established diagnostic criteria for SIH combining both clinical and radiological findings: i) any type of headache fulfilling the following conditions: headache developed in relation to decrease of CSF pressure; or CSF leakage; or headache leading to the discovery of CSF leak; ii) CSF pressure <6 cm H_20 or/and imaging findings of CSF leak; iii) is not attributed to any other ICHD-III diagnosis [78].

The pathophysiological mechanism explained by Monro-Kellie doctrine may help understand the imaging findings of IH [79]. The main imaging findings of IH reflect the alteration of the equilibrium between CSF volume, intracranial blood and brain tissue. Since the brain tissue volume is stable, a decrease in CSF volume will be followed by compensatory increase of intracranial blood. These changes thus, result into

Figure 8. On axial FLAIR images, in a 26-year-old patient with family history of cerebral autosomal dominant arteriopathy with subcortical infarcts and leukoencephalopathy (CADASIL), widespread white matter hyperintensities most pronounced in the temporal lobes are demonstrated. The thalami and pons are also affected

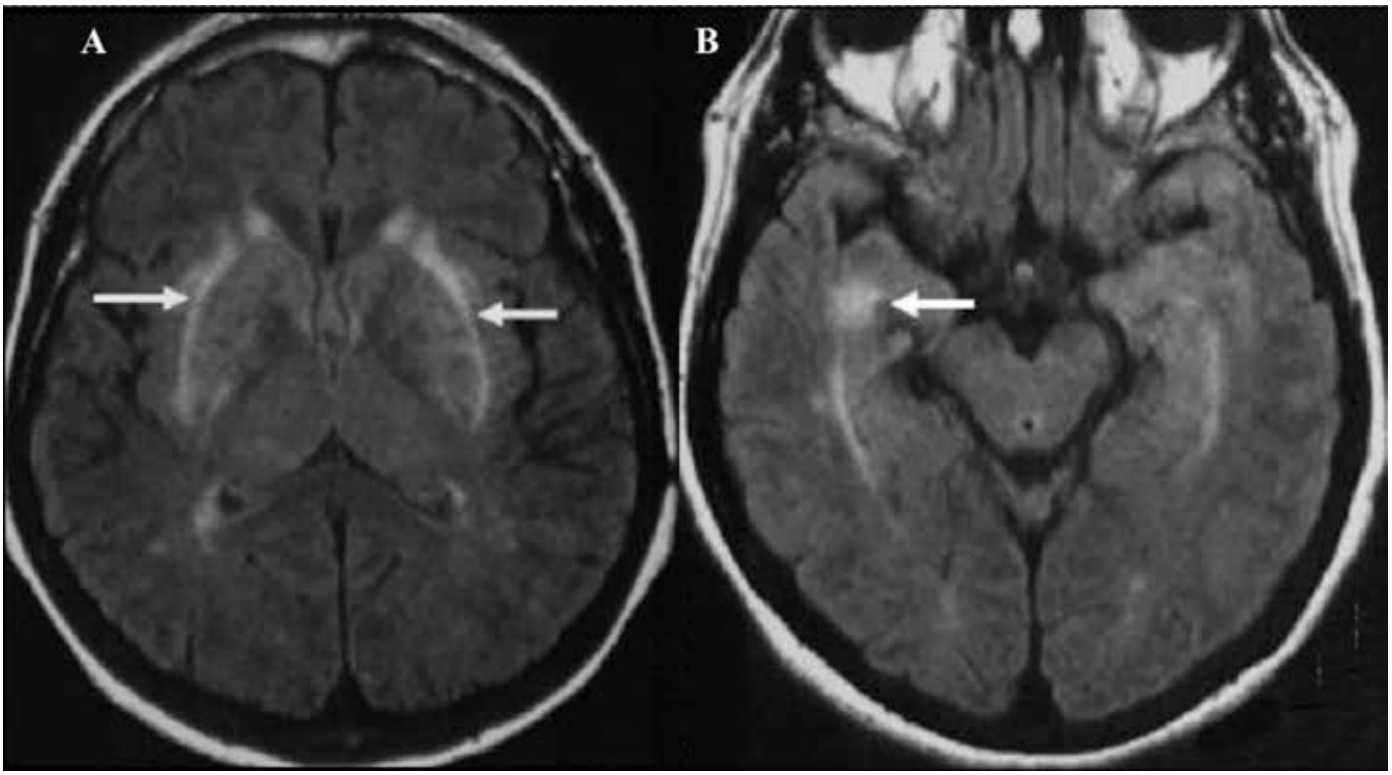

dilatation of vascular spaces, specifically the venous spaces due to their higher compliance [80].

Brain CT can be a helpful tool for the initial diagnosis of IH in the ER as well as in the outpatient setting [78]. Nevertheless, the imaging method of choice for IH diagnosis and treatment monitoring is brain MRI, while intravenous contrast administration is mandatory to depict the typical IH features. It should be noted, that brain imaging may be normal in approximately 20-30% of patients with clinically confirmed diagnosis according to the aforementioned diagnostic criteria proposed by ICHD-3 [78, 81]. Complementary whole spine MRI with intravenous contrast administration has been recommended in patients unresponsive to medical treatment to identify IH and potentially to depict the site of CSF leakage. Although spine MRI can detect in some case the location of CSF leak, CT myelography (CTM) is more sensitive for leak identification [82].Conventional myelography must be performed either when a rapid leak is suspected, which may be obscured on CTM, or when CTM findings are normal. Invasive MR myelography with intrathecal gadolinium administration has a higher sensitivity than CTM for CSF leak depiction, but the intrathecal use of gadolinium still remains off-label [83-85].

During the past years, CSF flow studies on MRI have been increasingly used to assess and quantify pulsatile CSF flow. 2D phase-contrast MRI (PC-MRI) is the most widely used velocity encoding method for CSF flow analysis. Typically, the CSF flow parameters obtained with PC-MRI are significantly lower in IH patients compared to healthy controls (Figures 9, 10) [86]. Moreover, a correlation has been established between CSF flow parameters, headache intensity and CSF opening pressure [86]. Similarly, PC-MRI parameters in patients with spontaneous IH may be used for treatment follow-up [87].

Diffuse pachymeningeal thickening and enhancement is the most common MRI finding in IH patients. The thickening and enhancement is typically smooth and continuous without skip areas. The aforementioned imaging findings are attributed to "leaky" dural microvessels, which have been shown to lack tight connections and enable "spilling" of gadolinium [88]. It should also be mentioned that diffuse pachymeningeal thickening may not be evident in chronic IH cases, which in conjunction with changes in clinical findings (i.e., alteration of the headache pattern) may hinder IH diagnosis [89]. Another common imaging feature in IH patients, affecting approximately 50% of cases, is the presence of hyperintense subdural effusions due to the presence of proteinaceous fluid leaking from the congested dura [90]. Further imag-

Figure 9. A middle-aged female patient 5 days after sinus surgery presented with headache and fever. On axial FLAIR (A) and T1W (B) images, enlarged subdural collections and prominent dural thickening were evident, along with strong pachymeningeal enhancement on post-contrast T1W (C). On 2D phase-contrast MRI (PC-MRI) (D), the CSF flow metrics did not reveal any sign suggestive of intracranial hypotension

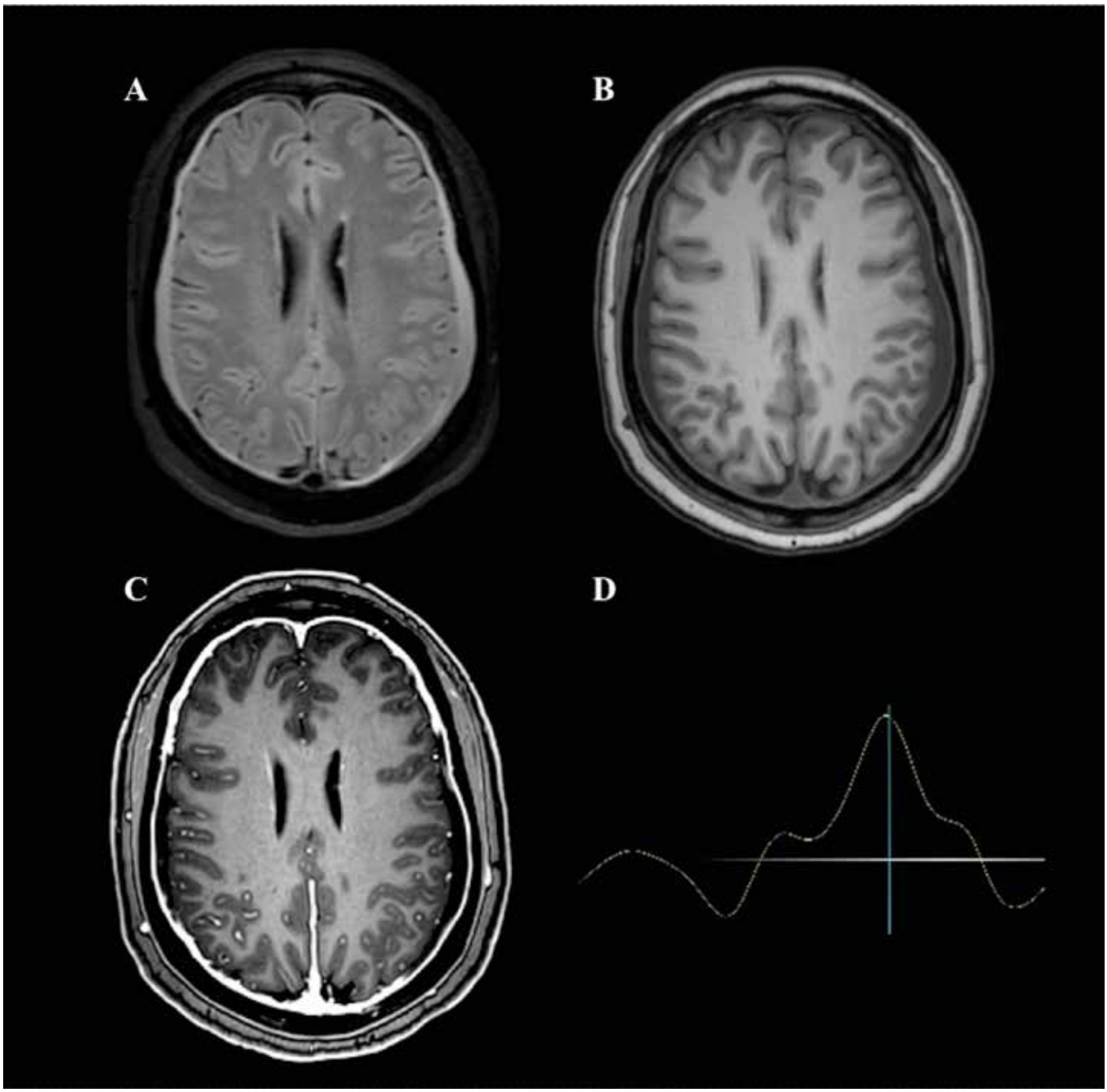

ing abnormalities include engorgement of venous structures, enlargement of the pituitary gland, caudal tonsillar displacement and slit ventricles [88].

Spinal MRI, in 67-100% of cases, will show fluid collections-spinal hygromas in the epidural space. Longitudinally, spinal hygromas typically exceed five spinal segments, and are located either anteriorly or posteriorly to the dural sac [91]. Other findings suggestive of IH include engorged spinal epidural veins, circumferential dural enhancement usually combined with intracranial dural enhancement and fluid between the C1-C2 spinous processes. The latter finding is attributed to transudate leakage from the rich regional venous plexus and is considered as a CSF "false-localizing" sign [91].

Figure 10. Spinal longitudinal extradural collections. (A), Sagittal T2 FSE. (B), Reformatted axial 3D-T2W images show spinal longitudinal extradural CSF collections (SLECs - arrows) and displaced dura outlined by the CSF. (C and D), Images similar to A and B of the same patient show similar findings in the lower thoracic region

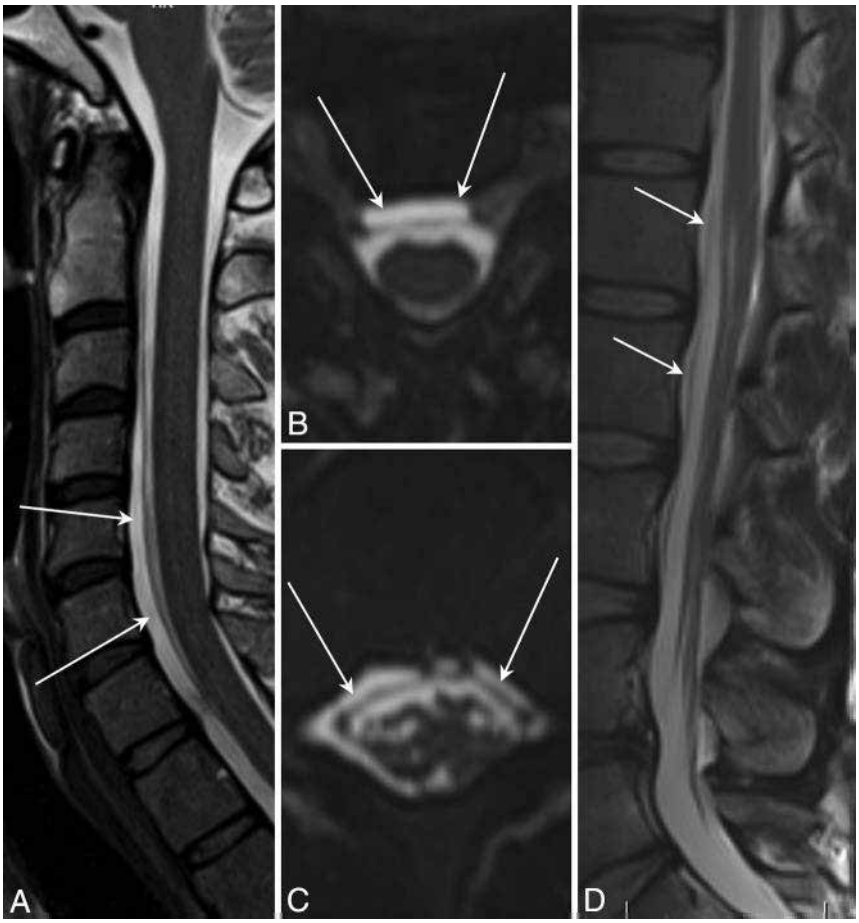

Idiopathic Intracranial hypertension (IIH)

IIH, previously known as pseudotumor cerebri, comprises another cause of secondary headache, attributed to elevated intracranial pressure, without evident causative mass or hydrocephalus. Typically, there is a female predominance, with IIH affecting mostly women of reproductive age, with increased body mass index. The most common presenting symptom of IIH is a pressure-like, throbbing headache. Additional clinical symptoms include transient visual obscuration with typical tunnel vision, photopsia, eye pain, pulsatile tinnitus, rarely 6th cranial nerve palsy and papilledema, which warrants ophthalmological evaluation. When lumbar puncture is performed, the CSF composition is normal but the opening CSF pressure is in most cases increased (>20cm H_2O in normal weight patients and >25cm H_2O in obese patients) [92]. Revised diagnostic criteria for IIH have been proposed by Friedman et al. including both clinical and neuroimaging findings [93]. Neuroimaging must precede diagnostic lumbar puncture to exclude increased CSF pressure due to other causes, including brain tumor, dural sinus thrombosis, infection, hydrocephalus.

Structural MRI is the cornerstone for IIH diagnosis, which enables the exclusion of other underlying causes of elevated intracranial pressure, but also facilitates the identification of neuroimaging abnormalities characteristic for IIH. The main axes of neuroimaging should be tailored to assess the orbits and the intracranial compartment. Orbital changes comprise (i) prominent subarachnoid space around the optic nerves with vertical tortuosity, (ii) flattening of the posterior sclera followed by intraocular protrusion, and (iii) enhancement of the optic nerve head [94-96]. The majority of imaging findings in the intracranial cavity are associated with the enlargement of outpouchings of the arachnoid space. The most suggestive imaging findings of IIH intracranially are the 'empty sella' sign, depicted as loss of the midsagittal height of the pituitary gland, and the Meckel's cave enlargement, depicted as enlargement

Figure 11. 32-year-old female patient, complaining for headaches, with confirmed by lumbar puncture Idiopathic Intracranial Hypertension, demonstrating in sagittal (A) and coronal T2W (B), as well as in transverse FLAIR (C) images the classic "empty sella" sign, and the optic nerves with vertical tortuosity. No signs of arterial or venous sinuses thrombosis in MRA (D) and MRV (E). Normal values in whole brain Volumetric analysis (F). The patient was treated with acetazolamide, as she refused the neurosurgical shunting procedure

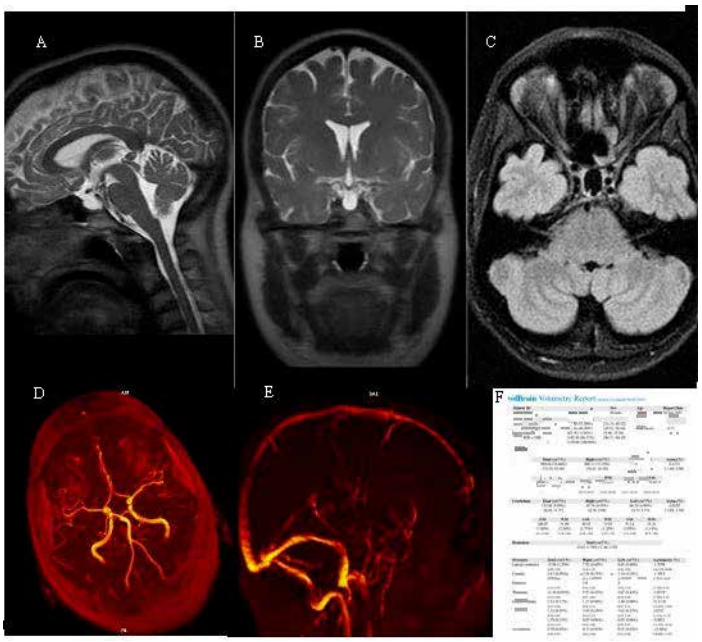

of the porus trigeminus notch accompanied by a smooth cystic space in the anteromedial petrous apex [97, 98].Semiautomated volumetric methods can quantitatively assess the volume of the optic nerve sheath and pituitary gland. Objective metrics derived from the volumetric assessment may be utilized both for the diagnosis and follow-up of IIH patients [99].

Another suggestive imaging feature of IIH occurring in 65-90% of cases is transverse sinus narrowing depicted on MR venography, which may require further investigation with contrast-enhanced 3D MR venography or invasive digital subtracted venography [100]. Other less common signs of IIH are slit-like ventricles and acquired tonsillar ectopia, which is a mimicker of Chiari Malformation Type 1 [101]. Phase-contrast cine magnetic resonance imaging (PCC-MRI) and derived CSF parameters have also been used as a non-invasive technique for IIH diagnosis and treatment follow-up [102] (Figure 11).

Chiari Malformation Type 1 (CM1)

The hallmark of Chiari Malformation Type 1 is the projection and downward displacement of the cerebellar tonsils through the foramen magnum. The clinical features of CM1 are proportional to the degree of tonsillar prolapse. Headache is a common presenting symptom of CM1, along with symptoms associated with brainstem compression / dysfunction, syringomyelia, or hydrocephalus [103]. Furthermore, it should be mentioned that Valsalva maneuver or cough can provoke headache in the setting of CM1. Low-lying tonsils (benign tonsillar ectopia) must be differentiated from CM1, with the former being asymptomatic and considered an incidental finding compatible with tonsillar protrusion of up to 3-5 mm through the foramen magnum.

The imaging modality of choice for the diagnosis of CM1 is MRI. The cerebral tonsillar position can be accurately assessed on MRI and the degree of caudal descent can be measured, preferably on midsagittal plane. The imaging signs supporting CM1 include pointed tonsils referred as 'peg-like' tonsils, vertically oriented sulci referred as 'UK sergeant stripes' and crowding of subarachnoid space at the level of craniocervical junction by tonsillar prolapse mainly observed on axial images (Figure 12) [104]. Measuring of the CSF flow with PC-MRI may be abnormal in cases of CM1 due to pulsatile motion of tonsils [105]. The imaging protocol should include spinal cord MRI in order to exclude the presence of syringomyelia, that may be evident in 40% of patients with CM1 [106].

Brain Tumour

As already mentioned, headache can be caused by any space-occupying brain lesion. The headache pattern caused by brain neoplasms varies and the

Figure 12. Cerebral tonsillar caudal descent through the foramen magnum attributed to Chiari Malformation Type I. (A) On sagittal image, the cerebellar tonsils are low-lying (>5mm) and appear 'peg like' and pointed. Cerebellar tonsillar position is the vertical distance (purple line) from the tip of the cerebellar tonsils to a line drawn between the anterior and posterior rims of the foramen magnum, known as McRae line (blue line). (B) On coronal image, the tonsillar caudal descent is depicted. (C) Axial image through the foramen shows crowding of the medulla by the tonsils. No syrinx was evident

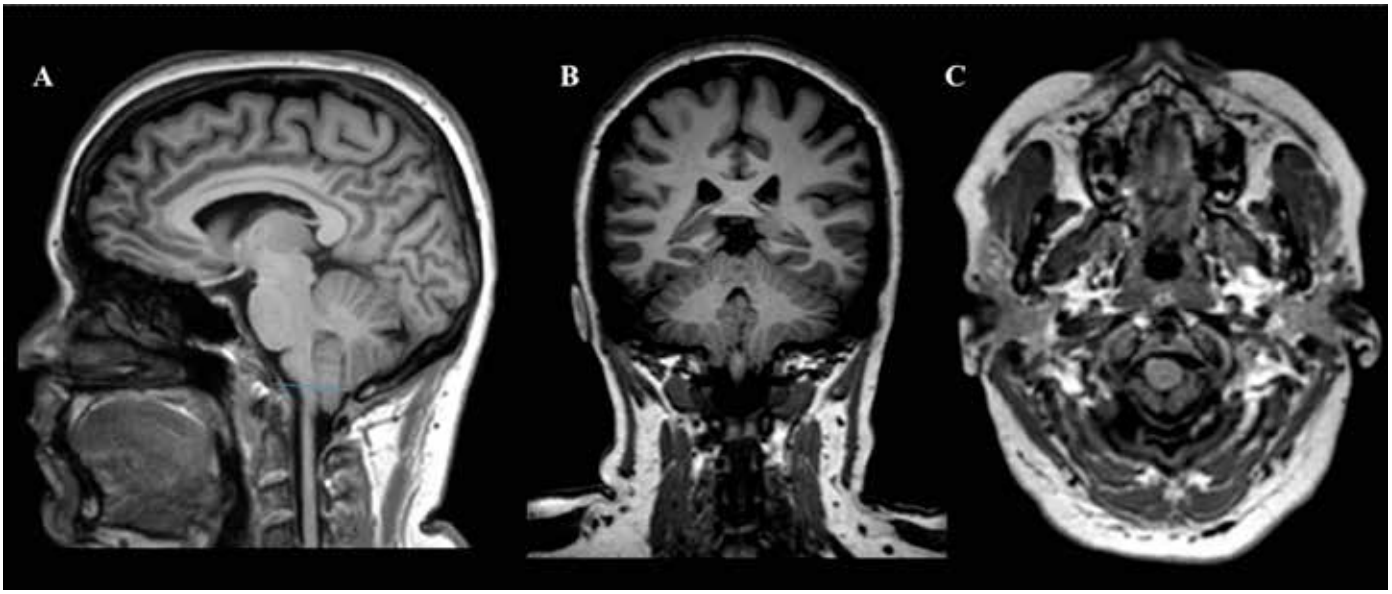

majority of patients presents with atypical findings [107]. Recently, advanced MRI techniques have radically changed the diagnostic approach to intracranial tumours. The WHO 2021 classification and grading of brain neoplasms has added more information about the phenotype of brain tumours and their genetic-molecular and genetic–prognostic correlations [108]. Conventional and advanced MRI techniques enable the diagnosis and staging of brain tumours, neurosurgical and radiotherapy planning, as well as treatment monitoring differentiating between pseudoprogression, progression or recurrence (Figures 13-16) [109].

Secondary headache attributed to infection

Brain Abscess

A cerebral abscess is a consequence of encephalitis and is typically characterized by accumulation of pus, which is surrounded by a capsule. Encephalitis and brain abscess can result from haematogenous dissemination (i.e., endocarditis), or as a complication of contiguous spread from paranasal sinuses, odontogenic or ear infection. Headache may be present in 69% of patients, but only 20% of them will suffer from the classic triad, which consists of headache, fever and focal neurologic deficits [110].

The pathogenesis of a brain abscess includes four distinct stages: early cerebritis (1-3 days), late cerebritis (4-9 days), early capsule formation (10-13 days) and late capsule formation (from 14 days onwards). Furthermore, five histological zones have been described, that can aid understanding of the neuroimaging findings: (1) a necrotic centre; (2) an external zone of accumulated inflammatory cells, macrophages and fibroblasts; (3) a capsule with dense collagen; and (4) peripheral astrogliosis and edema [111].

With respect to neuroimaging, CT scan is not as sensitive as MR, with 6% of cases having false negative CT-findings. CT scan is invaluable in the ER for assessment of the degree of brain edema [111]. Besides abscess diagnosis, both CT and MRI may be used to depict potential complications, including ventriculitis and CSF obstruction with secondary hydrocephalus. With respect to MRI studies, conventional MRI sequences can be combined with complementary advanced MRI techniques (MR spectroscopy) for obtaining information that may be suggestive of specific pathogens. The necrotic centre of an abscess will appear on MRI with high signal on T2W, a three-layered low-signal capsule on T2W and vivid capsule enhancement on T1W after gadolinium injection [112]. Beyond conventional imaging, the abscess cavity is depicted with high signal on DWI with corresponding low value on ADC map, due to the purulent content. Furthermore, MR-perfusion helps in differentiating a brain abscess with low regional cerebral blood volume (rCBV) from a brain tumor with necrotic part, which typically has high rCBV due to high vascularization. Despite the use of advanced imaging, however, diagnostic difficulties in differentiating between abscess and brain tumour

Figure 13. A 32-year-old male presented with headache and on MRI a space occupying lesion is depicted, mainly located on the left temporal lobe. On T1W image (A), the lesion shows inhomogeneous low signal with no evident enhancement on post contrast T1W (B). (C) On perfusion dynamic susceptibility contrast T2* (DSC-T2*) the relative cerebral blood volume (rCBV) ration was calculated 3.79, compatible with high grade brain tumor. (D) On TE=144ms single voxel MRS inside the lesion, increased concentrations of choline (Cho), creatine (Cr), lactate (Lac) and lipids (Lip) are depicted with Cho / Cr ratio of 1.35 and Cho / NAA 2.38. Furthermore, peaks of myoinositol (mI) are depicted, a finding that supports the differentiation of a lower-grade glioma into a higher-grade glioma. (E) Presurgical task-based functional MRI (TB-fMRI) and Resting-State fMRI (RS-fMRI) based on the Blood oxygenation level dependent (BOLD) phenomenon were acquired and the lateralization of hippocampal and language networks was left-sided. The lesion was in close proximity, distance <1cm, with the posterior part of the left upper temporal gyrus (Wernicke), but also with the primary auditory cortex. The distance of the lesion from the Broca's area (inferior frontal gyrus) was clearly bigger than 2cm. (E) On Diffusion tensor imaging tractography –DTI tractography– the lesion was in close proximity with, probably infiltrating, the posterior part of the left superior longitudinal (arcuate) fasciculus, the inferior longitudinal fasciculus and the inferior fronto-occipital fasciculus

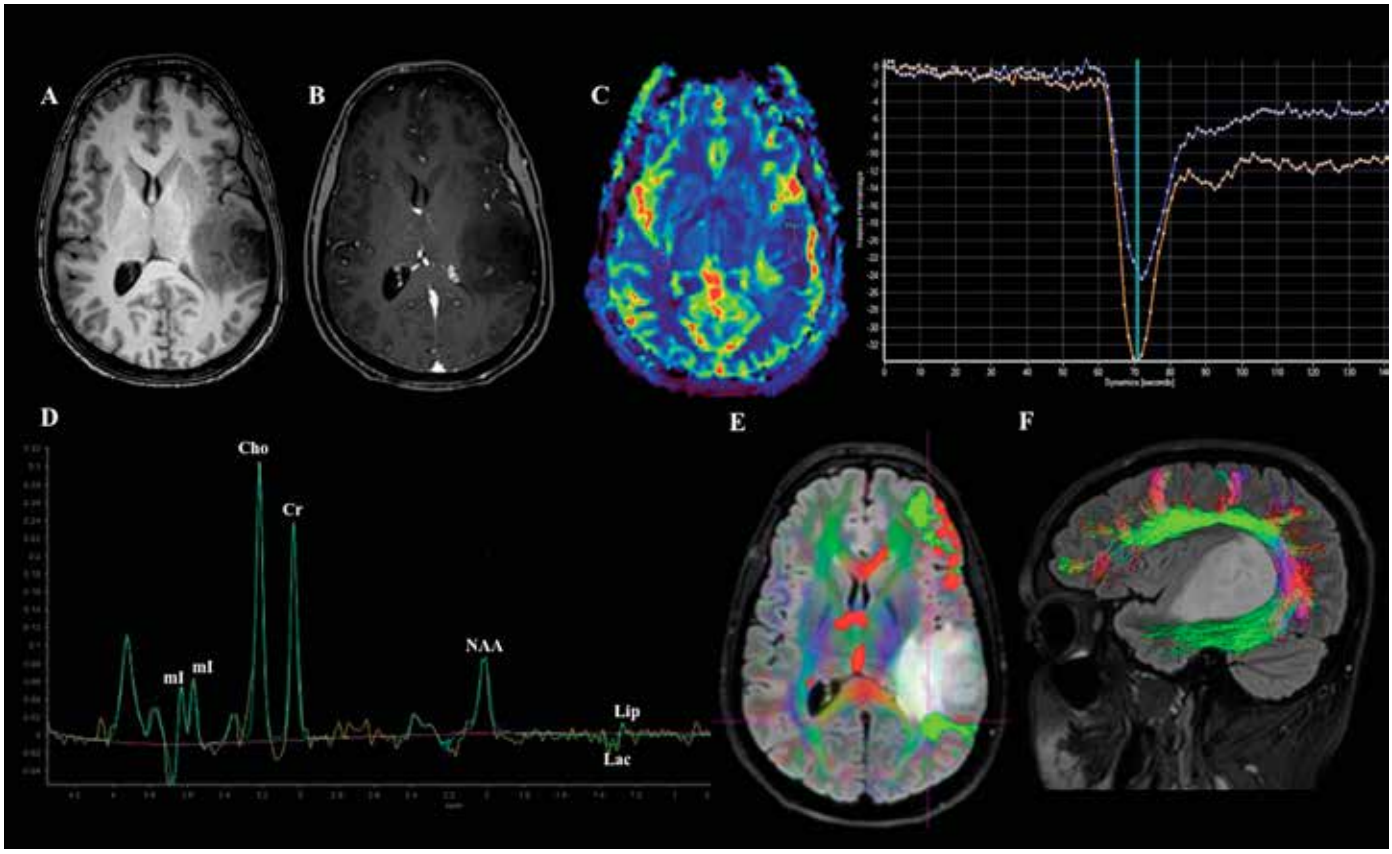

may arise in the early stages of capsule formation, when increased capillary density of the abscess may correspond to increased rCBV and lead to misdiagnosis [111].

MR Spectroscopy (MRS) is another advanced method widely performed for differential diagnosis of brain lesions that enables the delineation of their metabolic profile. MRS may show peaks of amino acids, lactate, lipids, succinate, acetate and alanine. The presence of peaks of amino acids is a sensitive marker of pyogenic abscess due to the breakdown of neutrophils inside the capsule, releasing proteolytic enzymes, which hydrolyse proteins into amino acids. However, absence of amino acids on MRS may be noted in patients with brain abscess who have undergone previous treatment with antibiotics. Furthermore, the peak of acetate with or without succinate on MRS has been described as a signature feature for anaerobic infection (Figures 17, 18) [113].

Headache or facial pain attributed to disorder of the cranium, neck, eyes, ears, nose, sinuses, teeth, mouth, or other facial or cervical structures

Rhinosinusitis

Rhinosinusitis can be divided in acute, subacute

Figure 14. Presurgical mapping in a 54-year-old patient presented with headache and neurological deficits. (A) Task-based functional MRI (TB-fMRI) with a paradigm of tongue movement revealed close proximity of the space occupying lesion and the corresponding cortical activation area of the tongue motion. (B) Inferior frontal gyrus (Broca's area) and superior temporal gyrus (Wernicke's area) activations in TB fMRI showed left-side lateralization of language. (C) Diffusion tensor imaging tractography depicted signs of probable infiltration of the right corticospinal tract and the right superior longitudinal fasciculus

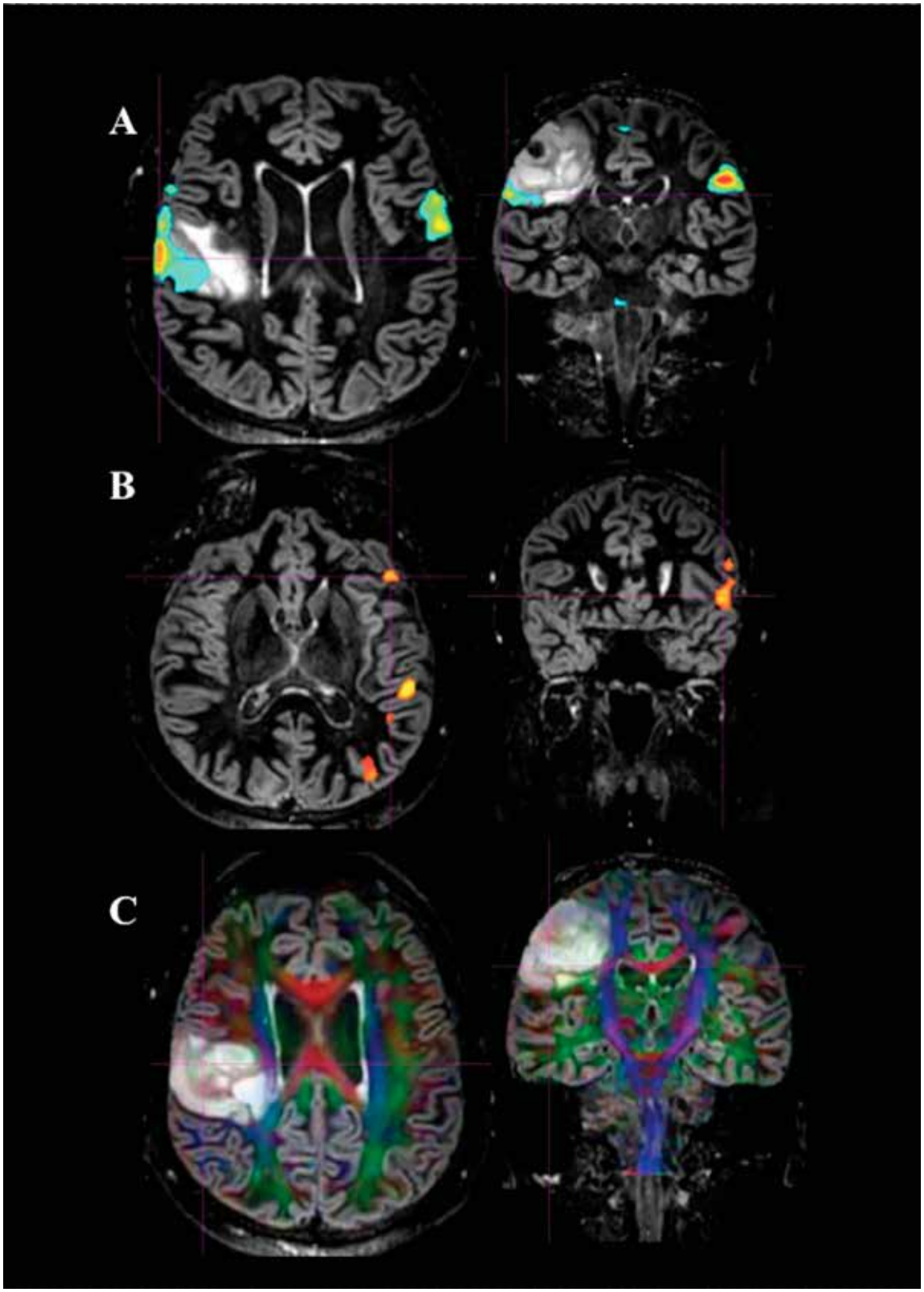

Figure 15. Artificial Intelligence (AI) segmentation for presurgical mapping and follow-up. (A) Presurgical AI anatomical segmentation map and volumetric assessment of enhancing tumor (pink-93.70ml), edema (blue-135.52ml) and necrosis (green-8ml) (B) Presurgical AI quantification based on perfusion dynamic susceptibility contrast T2* (DSC-T2*), for the description of vascular heterogeneity of the enhancing tumor and edema tissues in terms of the angiogenic process located at these regions. Red colour depicts high angiogenic enhancing tumor region-HAT (30.7ml), yellow colour depicts low angiogenic enhancing tumor region-LAT (45.55ml), green colour depicts potentially tumor infiltrated peripheral edema–IPE (28.86ml) and blue colour depicts pure vasogenic edema-VPE (82.75ml). (C) Post-surgery follow-up with AI segmentation maps and volumetric metrics (enhancing tumor-94.47ml, edema-133.21ml and necrosis-18ml). (D) Post-surgery follow-up AI with based on DSC-T2* quantification (HAT-22.88ml, LAT-54.04ml, IPE-25.61ml, VPE-83.44ml)

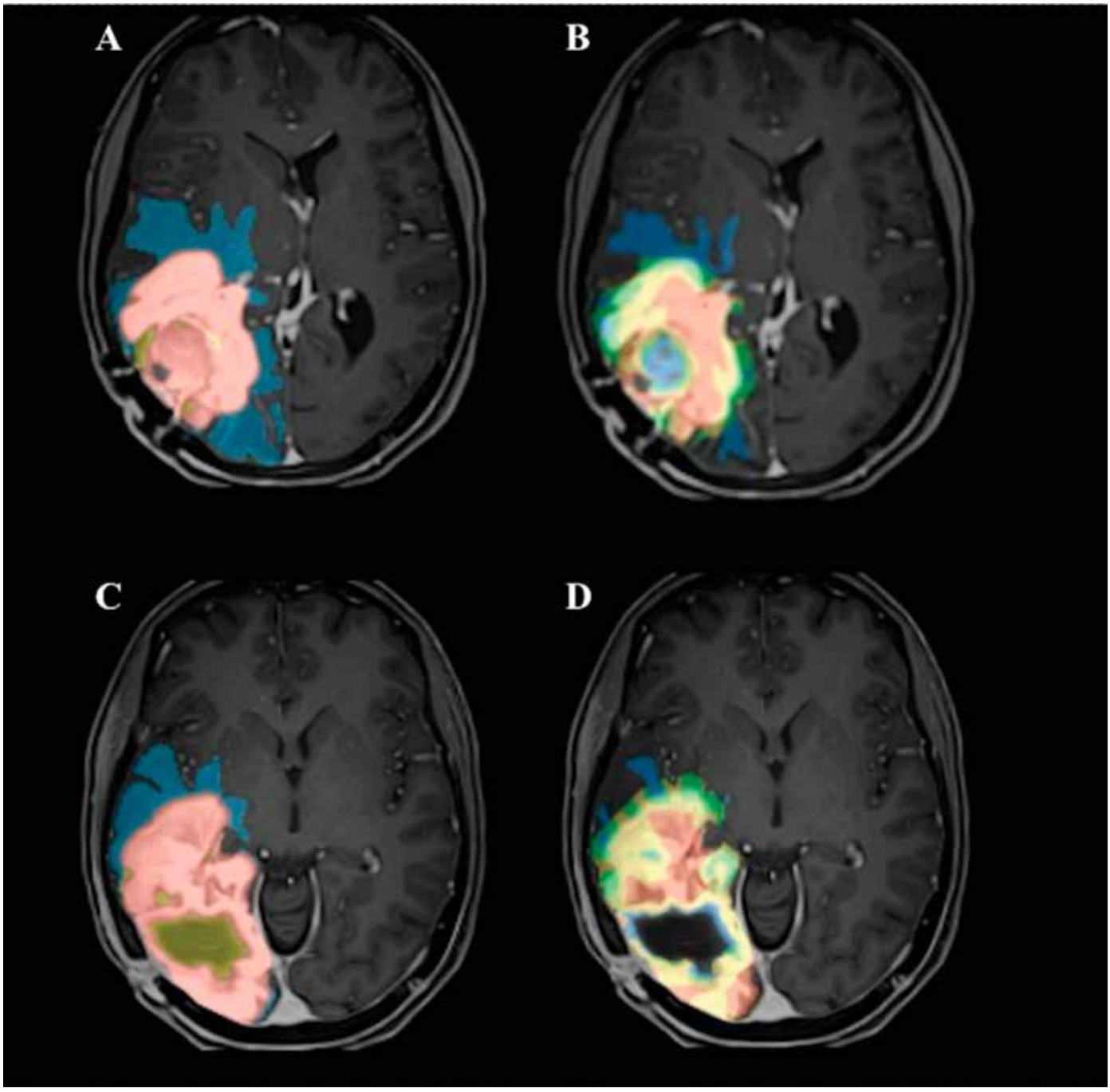

and chronic depending on the duration of symptoms. Headache is the most frequent clinical symptom of rhinosinusitis. With respect to neuroimaging, imaging findings of rhinosinusitis are non-specific and must always be correlated with evidence from clinical and/or endoscopic exams. It is noteworthy that 20-40%

Figure 16. DSC – T2* Perfusion MRI - based Fractional Tumor Burden (FTB) in the follow up of a glioblastoma multiforme patient with prior surgery and radio-chemo-therapy (red colour-rCBV>1.556 representing areas of high relative cerebral blood volume (rCBV), purple colour- 1<rCBV<1.556 representing areas with mild increased rCBV, blue colour - rCBV<1 representing normal rCBV). (A) Signs of relapse were evident (red colour-58.8%). (B) On the left frontal lobe, no signs of residual tumor were evident after the second surgery, but a new lesion on the left occipital lobe was depicted. This lesion consisted with 74.7% with rCBV>1.556, 20.8% with 1<rCBV<1.556 and 4.4% with rCBV<1. (C) Follow-up MRI after the third surgery did not reveal signs of residual tumor or relapse. (D) On follow-up MRI post-radiotherapy and post-chemotherapy, a new lesion on the left temporal lobe was depicted with 58.9% of rCBV>1.556

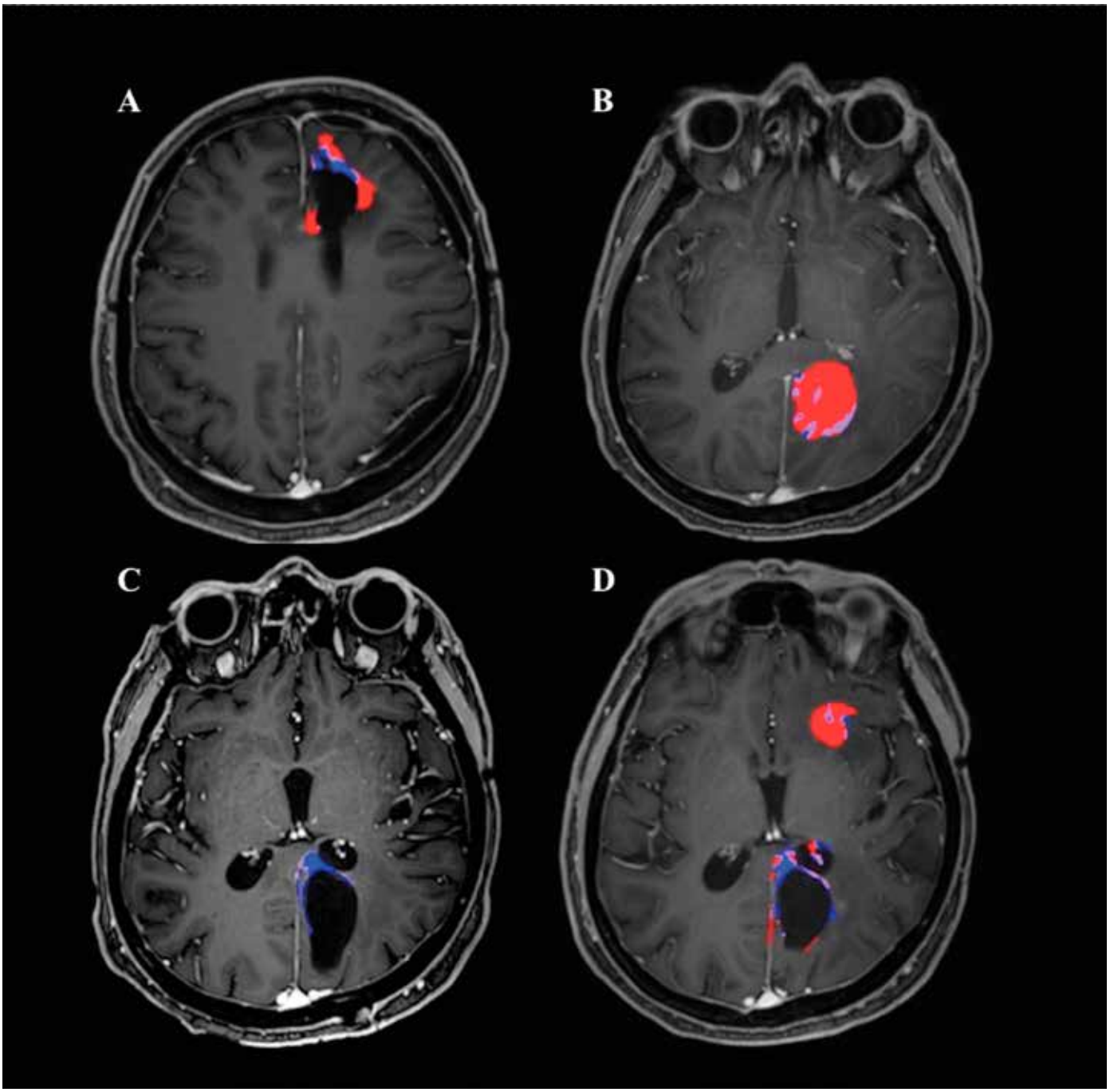

of patients undergoing MRI for any indication may incidentally show imaging abnormalities suggestive of rhinosinusitis [114]. Plain radiographs are part of the initial work up but have some limitations in assessing the extent of the inflammation, the sphenoid sinuses and potential complications of rhinosinusitis. CT scan remains the imaging modality of choice for depicting sinonasal cavities with higher anatomical

Figure 17. A female, who underwent dental surgery complained for headache and fever. On axial FLAIR (A), a high-signal-intensity mass with a low-signal-intensity capsule was detected. Perilesional high-signal-intensity vasogenic edema was also noted. Furthermore, high-signal –intensity was also revealed inside the right lateral ventricle. On axial T1W image (B) the lesion showed low-signal-intensity and the right lateral ventricle showed intermediate/high-signal intensity. On T1W post contrast (C) ring-like enhancement of the lesion was detected, as well as contrast enhancement was noted on the wall of the right lateral ventricle. On DWI b=1000 (D) the centre of the lesion showed a high signal, as well as inside the right lateral ventricle, with low ADC values (E), reflecting diffusion restriction. On TE=144ms single voxel MR-Spectroscopy (F) peaks of lipids (Lip), lactate (Lac), amino acids and **acetate (Ac)** were evident. All the imaging findings were compatible with pyogenic abscess complicated with ventriculitis. Staphylococcus epidermis was shown as the pathogenic microorganism after surgical aspiration of the lesion

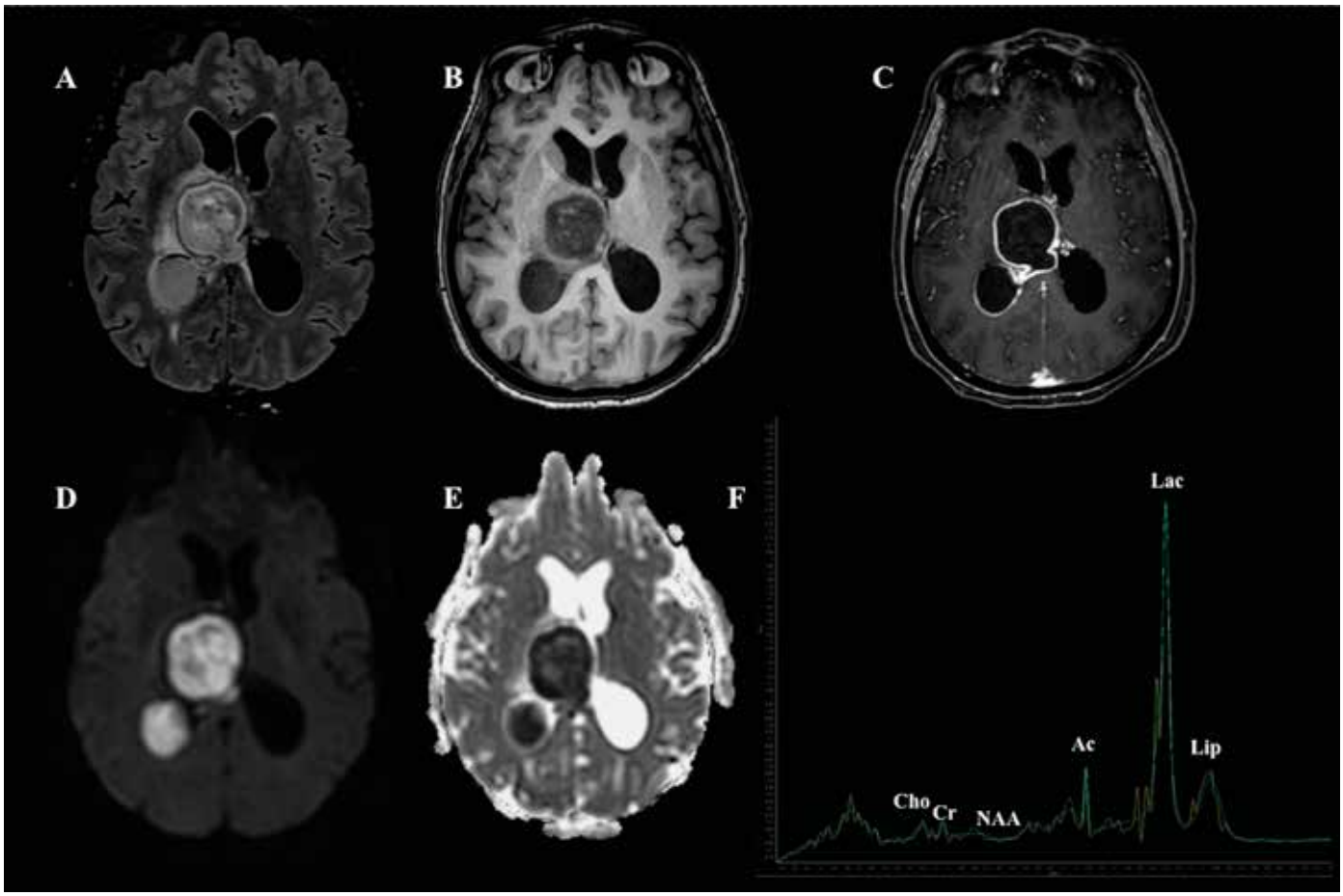

accuracy and can also be used as preoperative evaluation method [115]. Furthermore, CT scan is preferred for bone assessment, especially when chronic sinusitis is suspected. On the other hand, MRI has been suggested as the preferred imaging modality for evaluation of intracranial and orbital complications. Additionally, MRI is superior to CT for differentiating between inflammatory and neoplastic processes, while in case of a neoplasm MRI can also facilitate staging and surgery planning [116, 117].

Mucosal thickening along with presence of gas-fluid level and air bubbles within the paranasal sinuses are prominent on CT in acute rhinosinusitis, while when fungal infection is suspected, CT may reveal hyperdense lesions and probable calcifications within the paranasal sinuses [116, 118]. On T1 weighted images the mucosal thickening is isointense to soft tissue and the fluid is hypointense. On T2 weighted images both mucosal thickening and fluid will be hyperintense. On post contrast T1 weighted image only the inflamed mucosa will enhance in cases of acute rhinosinusitis or when acute and chronic rhinosinusitis concur (Figure 19). Bone sclerosis, rarefaction and periosteal reaction are best evaluated on CT scan and are considered hallmarks of chronic rhinosinusitis [116, 118].

Trigeminal Neuralgia (TN)

Trigeminal neuralgia (TN) belongs to the neuropathic facial pain syndromes and is defined according

Figure 18. A 66-year-old male patient with previous history of odontogenic infection presented with headache and neurological deficits along with fever and confusion. On MRI a space- occupying lesion on the left temporal lobe was detected. On T1W (A), the lesion showed inhomogeneous low signal with ring enhancement on post-contrast T1W (B). The central part of the lesion showed diffusion restriction with high signal on DWI b=1000(C) and low-signal on ADC map (D). On perfusion DSC T2* (H) the relative cerebral blood volume (rCBV) ratio was lower than 1.75. On intermediate TE=144ms single voxel MR-Spectroscopy (F) peaks of lipids (Lip), lactate (Lac), amino acids and *especially* acetate were evident. All the imaging findings and the patient history were suggestive of brain abscess, confirmed by surgical excision

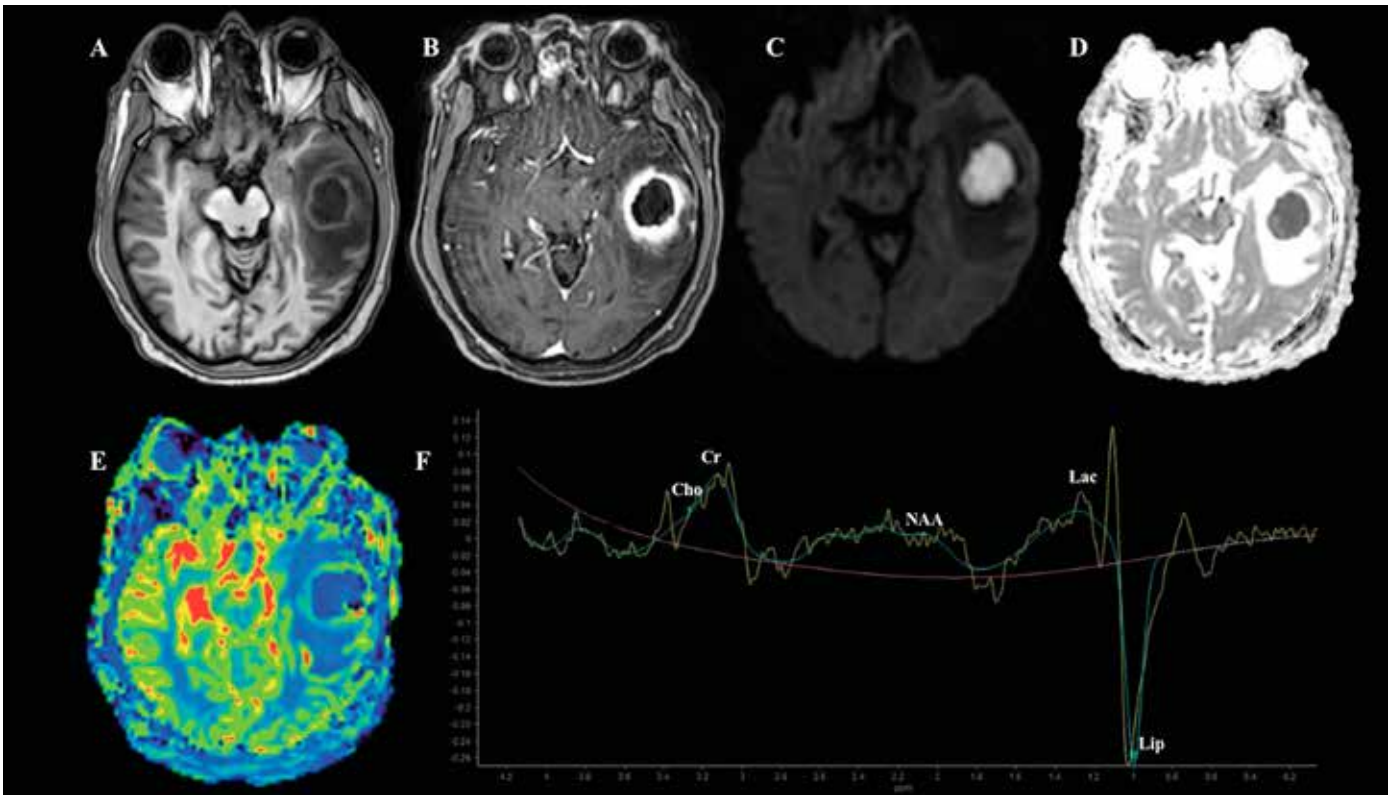

to the ICHD-III as unilateral distribution of a brief electric shock-like pain, limited to the distribution of one or more divisions of the trigeminal nerve [2, 119]. TN most frequently affects the maxillary or mandibular division of the trigeminal nerve. An innocuous stimulus may trigger the nerve abruptly. According to a recently proposed classification system, TN of unknown aetiology is categorized as idiopathic; TN caused by neurovascular compression is labelled as Classical TN; and TN associated with structural abnormalities (i.e., demyelinating lesions and neoplasms) is characterized as secondary TN [120].

- Classical TN

Classical TN is caused by a vascular loop, most commonly arterial, either deriving from the superior cerebellar artery or its branches, compressing the cisternal portion of the trigeminal nerve. Less commonly the vascular loop is formed by the transverse pontine vein, which compresses the trigeminal nerve [121]. The development of high-resolution 3D MRI sequences has increased the diagnostic sensitivity of vascular loop identification which may enable selection of patients that may benefit from microvascular decompressive surgery. Of note, that imaging findings suggestive of indentation of the trigeminal nerve by a vascular loop may be incidentalomas in patients undergoing MRI, but are far more common in symptomatic TN patients [122, 123]. GRE sequences and contrast-enhanced MRA can reveal the neurovascular contact at the root entry or exit zone of the trigeminal nerve on the affected side (Figure 20) [124]. Furthermore, some studies suggest that fractional anisotropy (FA) on diffusion-tensor imaging (DTI) is significantly lower at the affected side compared to the contralateral side [125, 126].

- TN secondary to Multiple Sclerosis (MS)

Patients with MS suffer from different types of neuropathic pain, among which TN is highly predominant. The prevalence of TN in patients with MS ranges from 1.4% to 4.9% [127] and the diagnosis of TN may precede the diagnosis of MS in some cases [128].

Figure 19. (A) On axial T1W, peripheral mucosal thickening in maxillary sinuses and ethmoidal cells is depicted along with the presence of fluid-air level and strong enhancement on post-contrast T1W (B), imaging finding suggestive of acute rhinosinusitis

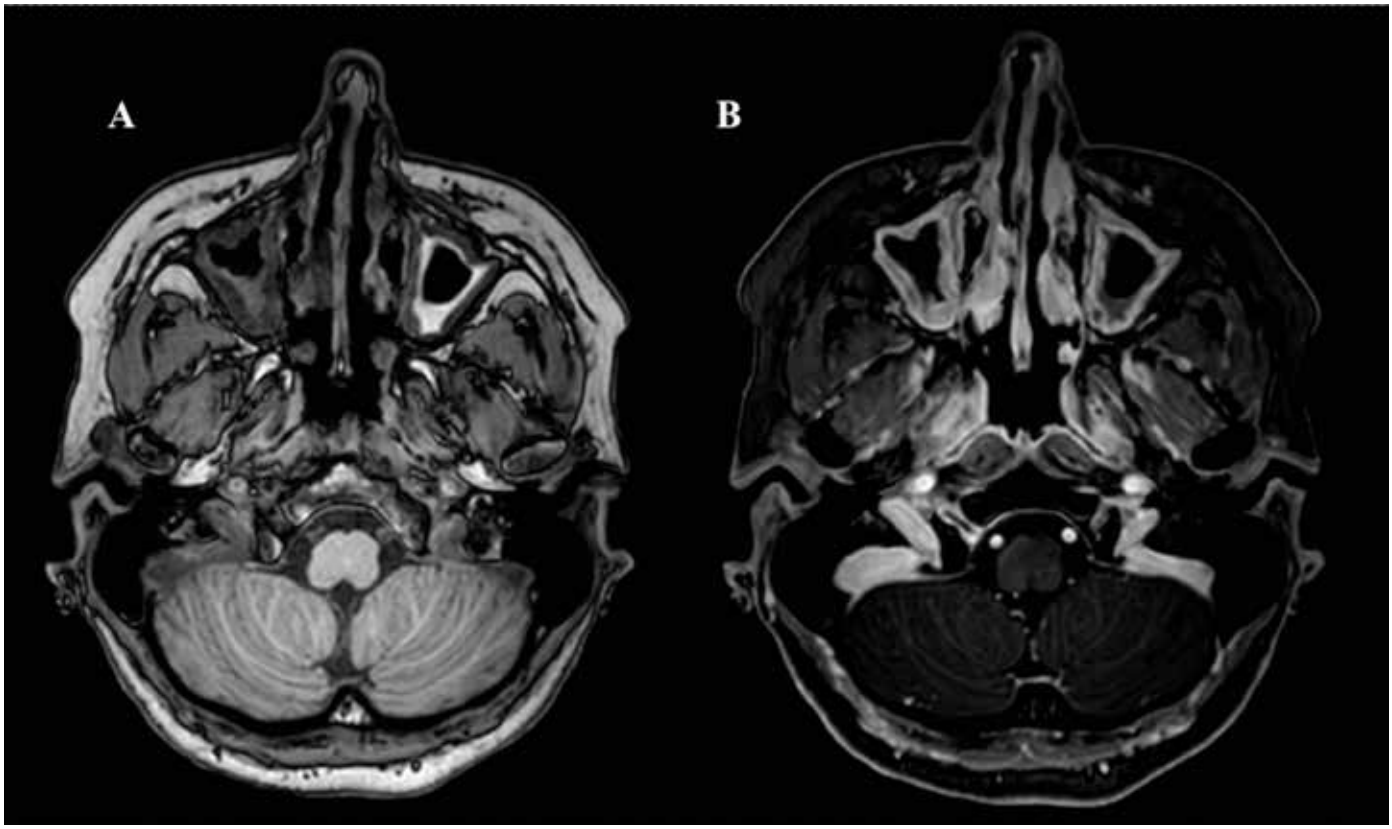

Figure 20. Right neurovascular compression by an arterial loop derived from the right superior cerebellar artery indenting the ipsilateral trigeminal nerve at its inferior surface with associated trigeminal nerve atrophy, depicted on heavily T2 weighted high-resolution axial image (A) and on MRA (B-axial, C-sagittal, D-coronal)

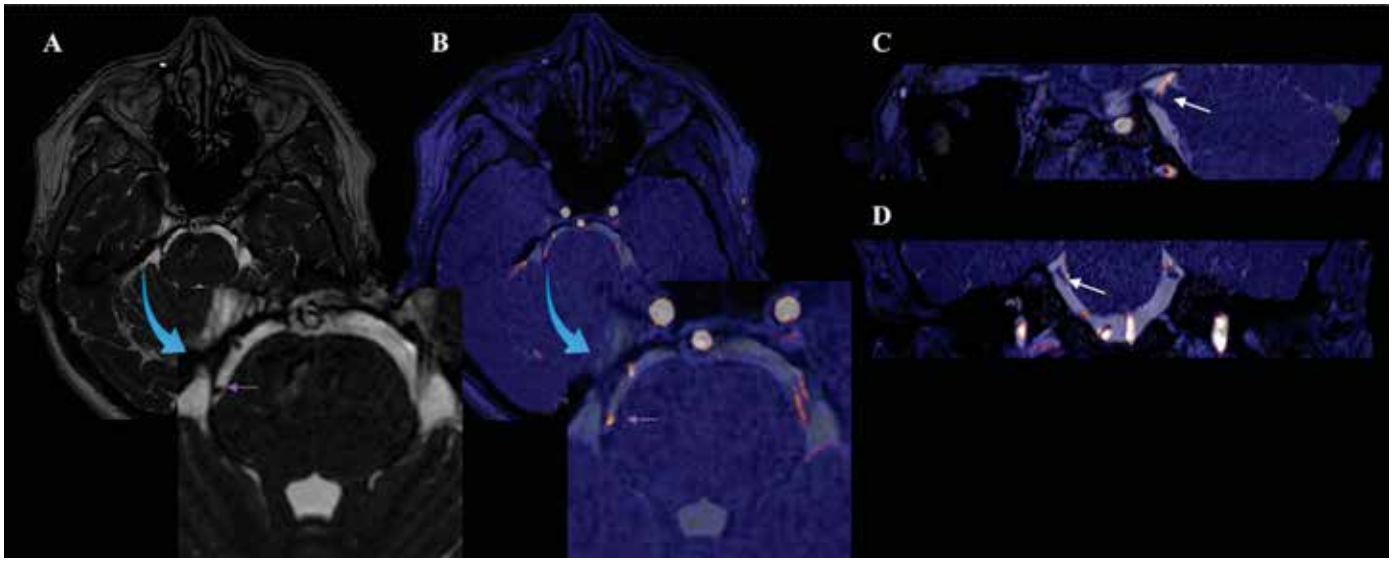

It has been established that TN secondary to MS is associated with the presence of a linear pontine demyelinating plaque involving the intrapontine segment of the trigeminal nerve, specifically in the area between the root entry zone and the nuclei [129].

The diagnosis of TN in patients with MS is based

Figure 21. A well-defined extra axial mass of the left trigeminal nerve is depicted at the left cerebellopontine angle cistern posteriorly to Meckel's cave. Balanced fast field-echo (BFFE) sequence provides detailed anatomical relationship between the mass and the left trigeminal nerve (A). On post-contrast T1 weighted image the lesion shows enhancement (B) with an estimated volume of 1.7441ml (C)

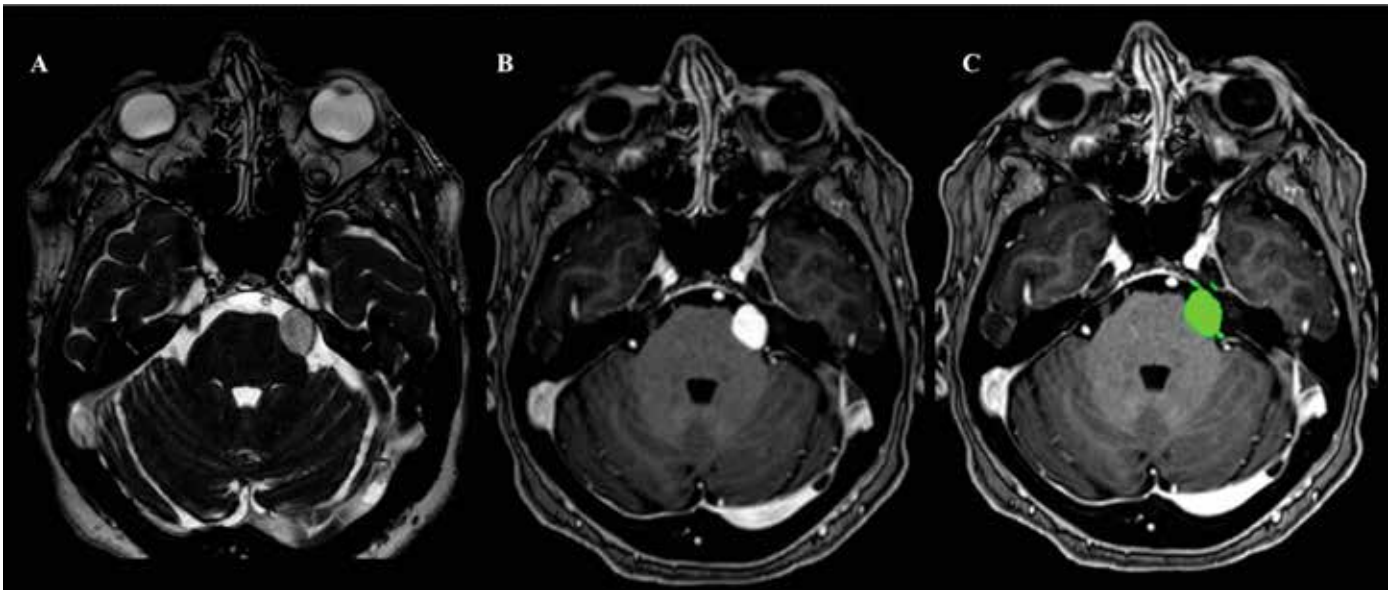

on neurophysiological techniques and MRI for the identification of trigeminal pathway impairment [120]. As MRI is routinely used for the diagnosis and follow-up of MS, a standardized MRI protocol has been suggested [130]. Therefore, in a patient with MS suffering from TN, besides MRI findings compatible with MS, a pontine lesion will be evident. This lesion will be more frequently unilateral, localized in the ventrolateral pons between the trigeminal root entry zone and the trigeminal nuclei, affecting the intrapontine part of primary afferents of the trigeminal nerve (Figure 21) [131].

- TN secondary to schwannoma

Trigeminal schwannoma is the second most common schwannoma following the vestibular schwannoma, mainly occurring in middle-aged adults, with a slight female preponderance. Trigeminal schwannomas are either sporadic or associated with neurofibromatosis type 2 (NF2). This type of schwannoma originates from nerve-sheath Schwann cells, therefore appears as a mass with well-defined margins abutting the nerve. If the schwannoma is confined in one compartment of the nerve it is subcategorized either as preganglionic (cisternal), ganglionic (confined to Meckel's cave) or postganglionic [132]. MRI establishes the location of the schwannoma, the approximate volume and its proximity to important anatomical structures, especially when surgical treatment is indicated. Imaging findings depend on the schwannoma size. Small schwannomas appear homogenously iso- or hypointense on T1- and T2-weighted images with avid enhancement after intravenous gadolinium administration. However, when they become larger, they show heterogeneous signal due to intratumoral necrosis or haemorrhage. Magnetic Resonance Cisternography is important for the proper assessment of the cisternal segment of the trigeminal nerve (Figure 22). CT scan is complementary to MRI in cases of bone erosions i.e., petrous apex erosion [133].

Quantitative MRI Volumetry and Dynamic Contrast-Enhanced (DCE) perfusion may be indicated for follow-up of trigeminal schwannoma after gamma knife stereotactic radiosurgery [134].

Conclusion

Headache is one of the most common clinical manifestations of neurological patients. Thorough neurological examination, recognition of red flags and worrisome features, as well as detailed patient history-taking help the clinician classify headache as primary or secondary, according to the ICDH-III. The optimal neuroimaging methods and protocols for headache diagnosis should be decided on an individual patient basis depending on the clinical suspicion of underlying headache causes. Overall, MRI is preferred for the delineation of underlying brain pathology in patients presenting with headache, with the exception of subarachnoid haemorrhage that necessitates performance of CT in the acute setting, as CT is characterized by higher sensitivity compared

Figure 22. A 74-years-old male with trigeminal neuralgia secondary to MS. On the axial (A), coronal (B) and sagittal (C) plane a pontine lesion in the left intrapontine fascicular part of the trigeminal nerve is noted (red colour) corresponding to a linear demyelinating plaque with associated trigeminal nerve atrophy. Images (A), (B) and (C) are derived after whole brain volumetric analysis using artificial intelligence and segmentation of grey, white matter, CSF and lesions. (D) Whole brain quantitative volumetry did not indicate brain atrophy, since the volume of the whole brain and grey matter are within the normal range for the age and sex of the examinee, while 1.4ml lesion load on FLAIR images were calculated with no enhancing lesion

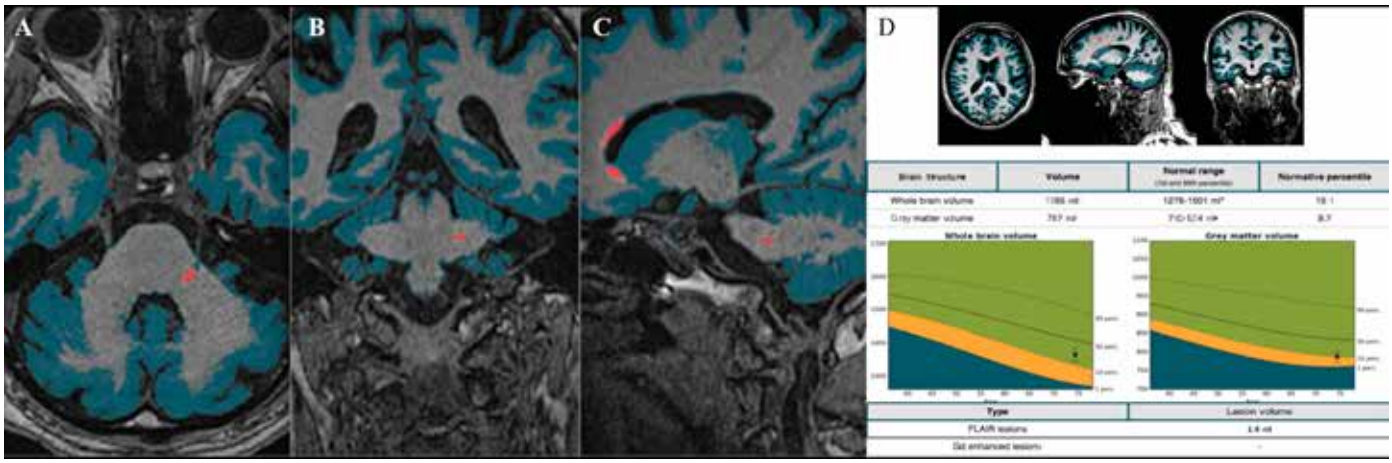

to MRI in the acute phase for detecting subarachnoid haemorrhage. In conclusion, conventional and advanced MRI techniques provide invaluable information regarding the underlying aetiology of secondary headaches and comprise indispensable tools in clinical practice for treatment planning and follow-up of patients suffering from secondary headache.

Conflicts of Interest Statement

The authors declare no conflicts of interest

References

[1] Olesen J. International Classification of Headache Disorders. Lancet Neurol. 2018;17(5):396-7.
[2] Headache Classification Committee of the International Headache Society (IHS). The International Classification of Headache Disorders, 3rd edition. Cephalalgia. 2018;38(1):1-211.
[3] Dodick DW. Clinical clues and clinical rules: primary vs secondary headache. Advanced Studies in Medicine. 2003;3(6 C):S550-S5.
[4] Loder E, Weizenbaum E, Frishberg B, Silberstein S. Choosing wisely in headache medicine: the American Headache Society's list of five things physicians and patients should question. Headache. 2013;53(10):1651-9.
[5] Carville S, Padhi S, Reason T, Underwood M. Diagnosis and management of headaches in young people and adults: summary of NICE guidance. Bmj. 2012;345:e5765.
[6] van Gijn J, Kerr RS, Rinkel GJ. Subarachnoid haemorrhage. Lancet. 2007;369(9558):306-18.
[7] May A, Straube A, Peikert A, Diener H. Diagnostik und apparative Zusatzuntersuchungen bei Kopfschmerzen. Leitlinien für Diagnostik und Therapie in der Neurologie. 2005;3:476-9.
[8] Jang YE, Cho EY, Choi HY, Kim SM, Park HY. Diagnostic Neuroimaging in Headache Patients: A Systematic Review and Meta-Analysis. Psychiatry Investig. 2019;16(6):407-17.
[9] Mitsikostas DD, Ashina M, Craven A, Diener HC, Goadsby PJ, Ferrari MD, et al. European Headache Federation consensus on technical investigation for primary headache disorders. J Headache Pain. 2015;17:5.
[10] Holle D, Obermann M. The role of neuroimaging in the diagnosis of headache disorders. Ther Adv Neurol Disord. 2013;6(6):369-74.
[11] Duncan C, Watson D, Stein A. Diagnosis and management of headache in adults: summary of SIGN guideline. Bmj. 2008;337.
[12] Sheikh HU. Headache in Intracranial and Cervical Artery Dissections. Curr Pain Headache Rep. 2016;20(2):8.
[13] Thanvi B, Munshi SK, Dawson SL, Robinson TG. Carotid and vertebral artery dissection syndromes. Postgrad Med J. 2005;81(956): 383-8.
[14] Tsivgoulis G, Mantatzis M, Vadikolias K, Heliopoulos I, Charalampopoulos K, Mitsoglou A, et al. Internal carotid artery dissection presenting as new-onset cluster headache. Neurol Sci. 2013;34(7):1251-2.

[15] Theodorou A, Palaiodimou L, Kokotis P, Papadopoulou M, Fradelos S, Voudouri A, et al. Teaching NeuroImages: An uncommon cause of carotid artery dissection: Fabry disease. Neurology. 2020;95(19):e2711-e3.
[16] Nebelsieck J, Sengelhoff C, Nassenstein I, Maintz D, Kuhlenbäumer G, Nabavi DG, et al. Sensitivity of neurovascular ultrasound for the detection of spontaneous cervical artery dissection. J Clin Neurosci. 2009;16(1):79-82.
[17] Ben Hassen W, Machet A, Edjlali-Goujon M, Legrand L, Ladoux A, Mellerio C, et al. Imaging of cervical artery dissection. Diagn Interv Imaging. 2014;95(12):1151-61.
[18] Rodallec MH, Marteau V, Gerber S, Desmottes L, Zins M. Craniocervical arterial dissection: spectrum of imaging findings and differential diagnosis. Radiographics. 2008;28(6):1711-28.
[19] Mehdi E, Aralasmak A, Toprak H, Yıldız S, Kurtcan S, Kolukisa M, et al. Craniocervical Dissections: Radiologic Findings, Pitfalls, Mimicking Diseases: A Pictorial Review. Curr Med Imaging Rev. 2018;14(2):207-22.
[20] Provenzale JM, Sarikaya B, Hacein-Bey L, Wintermark M. Causes of misinterpretation of cross-sectional imaging studies for dissection of the craniocervical arteries. AJR Am J Roentgenol. 2011;196(1):45-52.
[21] Provenzale JM, Sarikaya B. Comparison of test performance characteristics of MRI, MR angiography, and CT angiography in the diagnosis of carotid and vertebral artery dissection: a review of the medical literature. AJR Am J Roentgenol. 2009;193(4):1167-74.
[22] McNally JS, Hinckley PJ, Sakata A, Eisenmenger LB, Kim SE, De Havenon AH, et al. Magnetic Resonance Imaging and Clinical Factors Associated With Ischemic Stroke in Patients Suspected of Cervical Artery Dissection. Stroke. 2018;49(10):2337-44.
[23] Li Q, Wang J, Chen H, Gong X, Ma N, Gao K, et al. Characterization of Craniocervical Artery Dissection by Simultaneous MR Noncontrast Angiography and Intraplaque Hemorrhage Imaging at 3T. AJNR Am J Neuroradiol. 2015;36(9):1769-75.
[24] Wang J, Guan M, Yamada K, Hippe DS, Kerwin WS, Yuan C, et al. In Vivo Validation of Simultaneous Non-Contrast Angiography and intraPlaque Hemorrhage (SNAP) Magnetic Resonance Angiography: An Intracranial Artery Study. PLoS One. 2016;11(2):e0149130.
[25] Rodriguez-Valverde V, Sarabia JM, González-Gay MA, Figueroa M, Armona J, Blanco R, et al. Risk factors and predictive models of giant cell arteritis in polymyalgia rheumatica. Am J Med. 1997;102(4):331-6.
[26] Winkler A, True D. Giant Cell Arteritis: 2018 Review. Mo Med. 2018;115(5):468-70.
[27] Hernández-Rodríguez J, Murgia G, Villar I, Campo E, Mackie SL, Chakrabarty A, et al. Description and validation of histological patterns and proposal of a dynamic model of inflammatory infiltration in giant-cell arteritis. Medicine. 2016;95(8).
[28] Camellino D, Matteson EL, Buttgereit F, Dejaco C. Monitoring and long-term management of giant cell arteritis and polymyalgia rheumatica. Nat Rev Rheumatol. 2020;16(9):481-95.
[29] Bley TA, Uhl M, Carew J, Markl M, Schmidt D, Peter HH, et al. Diagnostic value of high-resolution MR imaging in giant cell arteritis. AJNR Am J Neuroradiol. 2007;28(9):1722-7.
[30] Rodriguez-Régent C, Ben Hassen W, Seners P, Oppenheim C, Régent A. 3D T1-weighted black-blood magnetic resonance imaging for the diagnosis of giant cell arteritis. Clin Exp Rheumatol. 2020;38 Suppl 124(2):95-8.
[31] Salvarani C, Brown RD, Jr., Calamia KT, Christianson TJ, Weigand SD, Miller DV, et al. Primary central nervous system vasculitis: analysis of 101 patients. Ann Neurol. 2007;62(5):442-51.
[32] Abdel Razek AA, Alvarez H, Bagg S, Refaat S, Castillo M. Imaging spectrum of CNS vasculitis. Radiographics. 2014;34(4):873-94.
[33] Mandell DM, Mossa-Basha M, Qiao Y, Hess CP, Hui F, Matouk C, et al. Intracranial Vessel Wall MRI: Principles and Expert Consensus Recommendations of the American Society of Neuroradiology. AJNR Am J Neuroradiol. 2017;38(2):218-29.
[34] Beuker C, Schmidt A, Strunk D, Sporns PB, Wiendl H, Meuth SG, et al. Primary angiitis of the central nervous system: diagnosis and treatment. Ther Adv Neurol Disord. 2018;11:1756286418785071.
[35] Stam J. Thrombosis of the cerebral veins and sinuses. N Engl J Med. 2005;352(17):1791-8.
[36] Ferro JM, Canhão P, Stam J, Bousser MG, Barinagarrementeria F. Prognosis of cerebral vein and dural sinus thrombosis: results of the International Study on Cerebral Vein and Dural Sinus Thrombosis (ISCVT). Stroke. 2004;35(3):664-70.
[37] Schwedt TJ, Matharu MS, Dodick DW. Thunderclap headache. Lancet Neurol. 2006;5(7):621-31.
[38] Slooter AJ, Ramos LM, Kappelle LJ. Migraine-like headache as the presenting symptom of cerebral venous sinus thrombosis. J Neurol. 2002;249(6):775-6.
[39] Botta R, Donirpathi S, Yadav R, Kulkarni GB, Kumar MV, Nagaraja D. Headache Patterns in Cerebral Venous Sinus Thrombosis. J Neurosci Rural Pract. 2017;8(Suppl 1):S72-s7.

[40] Ferro JM, Bousser MG, Canhão P, Coutinho JM, Crassard I, Dentali F, et al. European Stroke Organization guideline for the diagnosis and treatment of cerebral venous thrombosis - endorsed by the European Academy of Neurology. Eur J Neurol. 2017;24(10):1203-13.
[41] Leach JL, Fortuna RB, Jones BV, Gaskill-Shipley MF. Imaging of cerebral venous thrombosis: current techniques, spectrum of findings, and diagnostic pitfalls. Radiographics. 2006;26 Suppl 1:S19-41; discussion S2-3.
[42] Virapongse C, Cazenave C, Quisling R, Sarwar M, Hunter S. The empty delta sign: frequency and significance in 76 cases of dural sinus thrombosis. Radiology. 1987;162(3):779-85.
[43] Rodallec MH, Krainik A, Feydy A, Hélias A, Colombani J-M, Jullès M-C, et al. Cerebral venous thrombosis and multidetector CT angiography: tips and tricks. Radiographics. 2006;26(suppl_1):S5-S18.
[44] Macchi PJ, Grossman RI, Gomori JM, Goldberg HI, Zimmerman RA, Bilaniuk LT. High field MR imaging of cerebral venous thrombosis. J Comput Assist Tomogr. 1986;10(1):10-5.
[45] Saposnik G, Barinagarrementeria F, Brown RD, Jr., Bushnell CD, Cucchiara B, Cushman M, et al. Diagnosis and management of cerebral venous thrombosis: a statement for healthcare professionals from the American Heart Association/American Stroke Association. Stroke. 2011;42(4):1158-92.
[46] van Dam LF, van Walderveen MAA, Kroft LJM, Kruyt ND, Wermer MJH, van Osch MJP, et al. Current imaging modalities for diagnosing cerebral vein thrombosis - A critical review. Thromb Res. 2020;189:132-9.
[47] Poon CS, Chang JK, Swarnkar A, Johnson MH, Wasenko J. Radiologic diagnosis of cerebral venous thrombosis: pictorial review. AJR Am J Roentgenol. 2007;189(6 Suppl):S64-75.
[48] Arnoux A, Triquenot-Bagan A, Andriuta D, Wallon D, Guegan-Massardier E, Leclercq C, et al. Imaging characteristics of venous parenchymal abnormalities. Stroke. 2017;48(12):3258-65.
[49] Favrole P, Guichard J-P, Crassard I, Bousser M-G, Chabriat H. Diffusion-weighted imaging of intravascular clots in cerebral venous thrombosis. Stroke. 2004;35(1):99-103.
[50] deVeber G, Andrew M, Adams C, Bjornson B, Booth F, Buckley DJ, et al. Cerebral sinovenous thrombosis in children. N Engl J Med. 2001;345(6):417-23.
[51] Macdonald RL, Schweizer TA. Spontaneous subarachnoid haemorrhage. Lancet. 2017;389(10069):655-66.
[52] Flaherty ML, Haverbusch M, Kissela B, Kleindorfer D, Schneider A, Sekar P, et al. Perimesencephalic subarachnoid hemorrhage: incidence, risk factors, and outcome. J Stroke Cerebrovasc Dis. 2005;14(6):267-71.
[53] van der Schaaf IC, Velthuis BK, Gouw A, Rinkel GJ. Venous drainage in perimesencephalic hemorrhage. Stroke. 2004;35(7):1614-8.
[54] Sharma R, Dearaugo S, Infeld B, O'Sullivan R, Gerraty RP. Cerebral amyloid angiopathy: Review of clinico-radiological features and mimics. J Med Imaging Radiat Oncol. 2018.
[55] Korja M, Kivisaari R, Jahromi BR, Lehto H. Size and location of ruptured intracranial aneurysms: consecutive series of 1993 hospital-admitted patients. Journal of neurosurgery. 2016;127(4):748-53.
[56] Westerlaan HE, van Dijk JM, Jansen-van der Weide MC, de Groot JC, Groen RJ, Mooij JJ, et al. Intracranial aneurysms in patients with subarachnoid hemorrhage: CT angiography as a primary examination tool for diagnosis--systematic review and meta-analysis. Radiology. 2011;258(1):134-45.
[57] Lu L, Zhang LJ, Poon CS, Wu SY, Zhou CS, Luo S, et al. Digital subtraction CT angiography for detection of intracranial aneurysms: comparison with three-dimensional digital subtraction angiography. Radiology. 2012;262(2):605-12.
[58] da Rocha AJ, da Silva CJ, Gama HP, Baccin CE, Braga FT, Cesare Fde A, et al. Comparison of magnetic resonance imaging sequences with computed tomography to detect low-grade subarachnoid hemorrhage: Role of fluid-attenuated inversion recovery sequence. J Comput Assist Tomogr. 2006;30(2):295-303.
[59] Perry JJ, Stiell IG, Sivilotti ML, Bullard MJ, Emond M, Symington C, et al. Sensitivity of computed tomography performed within six hours of onset of headache for diagnosis of subarachnoid haemorrhage: prospective cohort study. Bmj. 2011;343:d4277.
[60] Okahara M, Kiyosue H, Yamashita M, Nagatomi H, Hata H, Saginoya T, et al. Diagnostic accuracy of magnetic resonance angiography for cerebral aneurysms in correlation with 3D-digital subtraction angiographic images: a study of 133 aneurysms. Stroke. 2002;33(7):1803-8.
[61] Mitchell P, Wilkinson ID, Hoggard N, Paley MN, Jellinek DA, Powell T, et al. Detection of subarachnoid haemorrhage with magnetic resonance imaging. J Neurol Neurosurg Psychiatry. 2001;70(2):205-11.
[62] van der Kleij LA, De Vis JB, Olivot JM, Calviere L, Cognard C, Zuithoff NP, et al. Magnetic Resonance Imaging and Cerebral Ischemia After Aneurysmal Subarachnoid Hemorrhage: A Systematic Review and Meta-Analysis. Stroke. 2017;48(1):239-45.

[63] Lad SP, Guzman R, Kelly ME, Li G, Lim M, Lovbald K, et al. Cerebral perfusion imaging in vasospasm. Neurosurgical Focus. 2006;21(3):1-9.
[64] Singhal AB, Hajj-Ali RA, Topcuoglu MA, Fok J, Bena J, Yang D, et al. Reversible cerebral vasoconstriction syndromes: analysis of 139 cases. Archives of neurology. 2011;68(8):1005-12.
[65] Singhal AB, Topcuoglu MA, Fok JW, Kursun O, Nogueira RG, Frosch MP, et al. Reversible cerebral vasoconstriction syndromes and primary angiitis of the central nervous system: clinical, imaging, and angiographic comparison. Annals of neurology. 2016;79(6):882-94.
[66] Miller T, Shivashankar R, Mossa-Basha M, Gandhi D. Reversible cerebral vasoconstriction syndrome, part 2: diagnostic work-up, imaging evaluation, and differential diagnosis. American Journal of Neuroradiology. 2015;36(9):1580-8.
[67] Mandell D, Mossa-Basha M, Qiao Y, Hess C, Hui F, Matouk C, et al. Intracranial vessel wall MRI: principles and expert consensus recommendations of the American Society of Neuroradiology. American Journal of Neuroradiology. 2017;38(2):218-29.
[68] Ducros A. Reversible cerebral vasoconstriction syndrome. Lancet Neurol. 2012;11(10):906-17.
[69] Miller TR, Shivashankar R, Mossa-Basha M, Gandhi D. Reversible Cerebral Vasoconstriction Syndrome, Part 1: Epidemiology, Pathogenesis, and Clinical Course. AJNR Am J Neuroradiol. 2015;36(8):1392-9.
[70] Paraskevas GP, Stefanou MI, Constantinides VC, Bakola E, Chondrogianni M, Giannopoulos S, et al. CADASIL in Greece: Mutational spectrum and clinical characteristics based on a systematic review and pooled analysis of published cases. Eur J Neurol. 2021.
[71] Vikelis M, Papatriantafyllou J, Karageorgiou CE. A novel CADASIL-causing mutation in a stroke patient. Swiss Med Wkly. 2007;137(21-22):323-5.
[72] Vikelis M, Xifaras M, Mitsikostas DD. CADASIL: a short review of the literature and a description of the first family from Greece. Funct Neurol. 2006;21(2):77-82.
[73] Stojanov D, Vojinovic S, Aracki-Trenkic A, Tasic A, Benedeto-Stojanov D, Ljubisavljevic S, et al. Imaging characteristics of cerebral autosomal dominant arteriopathy with subcortical infarcts and leucoencephalopathy (CADASIL). Bosn J Basic Med Sci. 2015;15(1):1-8.
[74] Gunda B, Porcher R, Duering M, Guichard JP, Mawet J, Jouvent E, et al. ADC histograms from routine DWI for longitudinal studies in cerebral small vessel disease: a field study in CADASIL. PLoS One. 2014;9(5):e97173.
[75] Holtmannspötter M, Peters N, Opherk C, Martin D, Herzog J, Brückmann H, et al. Diffusion magnetic resonance histograms as a surrogate marker and predictor of disease progression in CADASIL: a two-year follow-up study. Stroke. 2005;36(12):2559-65.
[76] Molko N, Pappata S, Mangin JF, Poupon F, LeBihan D, Bousser MG, et al. Monitoring disease progression in CADASIL with diffusion magnetic resonance imaging: a study with whole brain histogram analysis. Stroke. 2002;33(12):2902-8.
[77] Schievink WI, Schwartz MS, Maya MM, Moser FG, Rozen TD. Lack of causal association between spontaneous intracranial hypotension and cranial cerebrospinal fluid leaks. J Neurosurg. 2012;116(4):749-54.
[78] Lin JP, Zhang SD, He FF, Liu MJ, Ma XX. The status of diagnosis and treatment to intracranial hypotension, including SIH. J Headache Pain. 2017;18(1):4.
[79] Mokri B. The Monro-Kellie hypothesis: applications in CSF volume depletion. Neurology. 2001;56(12):1746-8.
[80] Wu JW, Wang YF, Hseu SS, Chen ST, Chen YL, Wu YT, et al. Brain volume changes in spontaneous intracranial hypotension: Revisiting the Monro-Kellie doctrine. Cephalalgia. 2021;41(1):58-68.
[81] Pattichis AA, Slee M. CSF hypotension: A review of its manifestations, investigation and management. J Clin Neurosci. 2016;34:39-43.
[82] Kranz PG, Luetmer PH, Diehn FE, Amrhein TJ, Tanpitukpongse TP, Gray L. Myelographic Techniques for the Detection of Spinal CSF Leaks in Spontaneous Intracranial Hypotension. AJR Am J Roentgenol. 2016;206(1):8-19.
[83] Akbar JJ, Luetmer PH, Schwartz KM, Hunt CH, Diehn FE, Eckel LJ. The role of MR myelography with intrathecal gadolinium in localization of spinal CSF leaks in patients with spontaneous intracranial hypotension. AJNR Am J Neuroradiol. 2012;33(3):535-40.
[84] Chazen JL, Talbott JF, Lantos JE, Dillon WP. MR myelography for identification of spinal CSF leak in spontaneous intracranial hypotension. AJNR Am J Neuroradiol. 2014;35(10):2007-12.
[85] Patel M, Atyani A, Salameh JP, McInnes M, Chakraborty S. Safety of Intrathecal Administration of Gadolinium-based Contrast Agents: A Systematic Review and Meta-Analysis. Radiology. 2020;297(1):75-83.
[86] Hasiloglu ZI, Albayram S, Gorucu Y, Selcuk H, Cagil E, Erdemli HE, et al. Assessment of CSF flow dynamics using PC-MRI in spontaneous intracranial hypotension. Headache. 2012;52(5):808-19.
[87] Tung H, Liao YC, Wu CC, Chang MH, Chen CC, Chen PL, et al. Usefulness of phase-contrast

magnetic resonance imaging for diagnosis and treatment evaluation in patients with SIH. Cephalalgia. 2014;34(8):584-93.
[88] Kranz PG, Gray L, Malinzak MD, Amrhein TJ. Spontaneous Intracranial Hypotension: Pathogenesis, Diagnosis, and Treatment. Neuroimaging Clin N Am. 2019;29(4):581-94.
[89] Kranz PG, Amrhein TJ, Choudhury KR, Tanpitukpongse TP, Gray L. Time-Dependent Changes in Dural Enhancement Associated With Spontaneous Intracranial Hypotension. AJR Am J Roentgenol. 2016;207(6):1283-7.
[90] Limaye K, Samant R, Lee RW. Spontaneous intracranial hypotension: diagnosis to management. Acta Neurol Belg. 2016;116(2):119-25.
[91] Medina JH, Abrams K, Falcone S, Bhatia RG. Spinal imaging findings in spontaneous intracranial hypotension. AJR Am J Roentgenol. 2010;195(2):459-64.
[92] Lenck S, Radovanovic I, Nicholson P, Hodaie M, Krings T, Mendes-Pereira V. Idiopathic intracranial hypertension: The veno glymphatic connections. Neurology. 2018;91(11):515-22.
[93] Friedman DI, Liu GT, Digre KB. Revised diagnostic criteria for the pseudotumor cerebri syndrome in adults and children. Neurology. 2013;81(13):1159-65.
[94] Suzuki H, Takanashi J, Kobayashi K, Nagasawa K, Tashima K, Kohno Y. MR imaging of idiopathic intracranial hypertension. AJNR Am J Neuroradiol. 2001;22(1):196-9.
[95] Degnan AJ, Levy LM. Pseudotumor cerebri: brief review of clinical syndrome and imaging findings. AJNR Am J Neuroradiol. 2011;32(11):1986-93.
[96] Bidot S, Saindane AM, Peragallo JH, Bruce BB, Newman NJ, Biousse V. Brain Imaging in Idiopathic Intracranial Hypertension. J Neuroophthalmol. 2015;35(4):400-11.
[97] Malhotra A, Tu L, Kalra VB, Wu X, Mian A, Mangla R, et al. Neuroimaging of Meckel's cave in normal and disease conditions. Insights Imaging. 2018;9(4):499-510.
[98] Moreno-Ajona D, McHugh JA, Hoffmann J. An Update on Imaging in Idiopathic Intracranial Hypertension. Front Neurol. 2020;11:453.
[99] Hoffmann J, Schmidt C, Kunte H, Klingebiel R, Harms L, Huppertz HJ, et al. Volumetric assessment of optic nerve sheath and hypophysis in idiopathic intracranial hypertension. AJNR Am J Neuroradiol. 2014;35(3):513-8.
[100] Satti SR, Leishangthem L, Chaudry MI. Meta-Analysis of CSF Diversion Procedures and Dural Venous Sinus Stenting in the Setting of Medically Refractory Idiopathic Intracranial Hypertension. AJNR Am J Neuroradiol. 2015;36(10):1899-904.
[101] Aiken AH, Hoots JA, Saindane AM, Hudgins PA. Incidence of cerebellar tonsillar ectopia in idiopathic intracranial hypertension: a mimic of the Chiari I malformation. AJNR Am J Neuroradiol. 2012;33(10):1901-6.
[102] Belal T, Al Tantawy A-E, Sherif FM, Ramadan A. Evaluation of cerebrospinal fluid flow dynamic changes in patients with idiopathic intracranial hypertension using phase contrast cine MR imaging. The Egyptian Journal of Neurology, Psychiatry and Neurosurgery. 2020;56(1):1-6.
[103] Langridge B, Phillips E, Choi D. Chiari Malformation Type 1: A Systematic Review of Natural History and Conservative Management. World Neurosurg. 2017;104:213-9.
[104] Chiapparini L, Saletti V, Solero CL, Bruzzone MG, Valentini LG. Neuroradiological diagnosis of Chiari malformations. Neurol Sci. 2011;32 Suppl 3:S283-6.
[105] Hofkes SK, Iskandar BJ, Turski PA, Gentry LR, McCue JB, Haughton VM. Differentiation between symptomatic Chiari I malformation and asymptomatic tonsilar ectopia by using cerebrospinal fluid flow imaging: initial estimate of imaging accuracy. Radiology. 2007;245(2):532-40.
[106] Elster AD, Chen MY. Chiari I malformations: clinical and radiologic reappraisal. Radiology. 1992;183(2):347-53.
[107] Schankin CJ, Ferrari U, Reinisch VM, Birnbaum T, Goldbrunner R, Straube A. Characteristics of brain tumour-associated headache. Cephalalgia. 2007;27(8):904-11.
[108] Louis DN, Perry A, Wesseling P, Brat DJ, Cree IA, Figarella-Branger D, et al. The 2021 WHO Classification of Tumors of the Central Nervous System: a summary. Neuro Oncol. 2021;23(8):1231-51.
[109] Iv M, Bisdas S. Neuroimaging in the Era of the Evolving WHO Classification of Brain Tumors, From the AJR Special Series on Cancer Staging. AJR Am J Roentgenol. 2021;217(1):3-15.
[110] Foerster BR, Thurnher MM, Malani PN, Petrou M, Carets-Zumelzu F, Sundgren PC. Intracranial infections: clinical and imaging characteristics. Acta Radiol. 2007;48(8):875-93.
[111] Rath TJ, Hughes M, Arabi M, Shah GV. Imaging of cerebritis, encephalitis, and brain abscess. Neuroimaging Clin N Am. 2012;22(4):585-607.
[112] Villanueva-Meyer JE, Cha S. From Shades of Gray to Microbiologic Imaging: A Historical Review of Brain Abscess Imaging: RSNA Centennial Article. Radiographics. 2015;35(5):1555-62.
[113] Pal D, Bhattacharyya A, Husain M, Prasad KN, Pandey CM, Gupta RK. In vivo proton

MR spectroscopy evaluation of pyogenic brain abscesses: a report of 194 cases. AJNR Am J Neuroradiol. 2010;31(2):360-6.
[114] Kamalian S, Avery L, Lev MH, Schaefer PW, Curtin HD, Kamalian S. Nontraumatic Head and Neck Emergencies. Radiographics. 2019;39(6):1808-23.
[115] Cashman EC, Macmahon PJ, Smyth D. Computed tomography scans of paranasal sinuses before functional endoscopic sinus surgery. World J Radiol. 2011;3(8):199-204.
[116] Mafee MF, Tran BH, Chapa AR. Imaging of rhinosinusitis and its complications: plain film, CT, and MRI. Clin Rev Allergy Immunol. 2006;30(3):165-86.
[117] Gregurić T, Prokopakis E, Vlastos I, Doulaptsi M, Cingi C, Košec A, et al. Imaging in chronic rhinosinusitis: A systematic review of MRI and CT diagnostic accuracy and reliability in severity staging. J Neuroradiol. 2021;48(4):277-81.
[118] Aribandi M, McCoy VA, Bazan C, 3rd. Imaging features of invasive and noninvasive fungal sinusitis: a review. Radiographics. 2007;27(5):1283-96.
[119] Headache Classification Committee of the International Headache Society (IHS). The International Classification of Headache Disorders, 3rd edition (beta version). Cephalalgia. 2013;33(9):629-808.
[120] Cruccu G, Finnerup NB, Jensen TS, Scholz J, Sindou M, Svensson P, et al. Trigeminal neuralgia: New classification and diagnostic grading for practice and research. Neurology. 2016;87(2):220-8.
[121] Sindou M, Brinzeu A. Topography of the pain in classical trigeminal neuralgia: insights into somatotopic organization. Brain. 2020;143(2):531-40.
[122] Jani RH, Hughes MA, Gold MS, Branstetter BF, Ligus ZE, Sekula RF, Jr. Trigeminal Nerve Compression Without Trigeminal Neuralgia: Intraoperative vs Imaging Evidence. Neurosurgery. 2019;84(1):60-5.
[123] Ruiz-Juretschke F, González-Quarante LH, García-Leal R, Martínez de Vega V. Neurovascular Relations of the Trigeminal Nerve in Asymptomatic Individuals Studied with High-Resolution Three-Dimensional Magnetic Resonance Imaging. Anat Rec (Hoboken). 2019;302(4):639-45.
[124] Hughes MA, Frederickson AM, Branstetter BF, Zhu X, Sekula RF, Jr. MRI of the Trigeminal Nerve in Patients With Trigeminal Neuralgia Secondary to Vascular Compression. AJR Am J Roentgenol. 2016;206(3):595-600.
[125] Lutz J, Linn J, Mehrkens JH, Thon N, Stahl R, Seelos K, et al. Trigeminal neuralgia due to neurovascular compression: high-spatial-resolution diffusion-tensor imaging reveals microstructural neural changes. Radiology. 2011;258(2):524-30.
[126] Zhang F, Xie G, Leung L, Mooney MA, Epprecht L, Norton I, et al. Creation of a novel trigeminal tractography atlas for automated trigeminal nerve identification. Neuroimage. 2020;220:117063.
[127] Foley PL, Vesterinen HM, Laird BJ, Sena ES, Colvin LA, Chandran S, et al. Prevalence and natural history of pain in adults with multiple sclerosis: systematic review and meta-analysis. Pain. 2013;154(5):632-42.
[128] Fallata A, Salter A, Tyry T, Cutter GR, Marrie RA. Trigeminal Neuralgia Commonly Precedes the Diagnosis of Multiple Sclerosis. Int J MS Care. 2017;19(5):240-6.
[129] Di Stefano G, Maarbjerg S, Truini A. Trigeminal neuralgia secondary to multiple sclerosis: from the clinical picture to the treatment options. J Headache Pain. 2019;20(1):20.
[130] Saslow L, Li DKB, Halper J, Banwell B, Barkhof F, Barlow L, et al. An International Standardized Magnetic Resonance Imaging Protocol for Diagnosis and Follow-up of Patients with Multiple Sclerosis: Advocacy, Dissemination, and Implementation Strategies. Int J MS Care. 2020;22(5):226-32.
[131] Swinnen C, Lunskens S, Deryck O, Casselman J, Vanopdenbosch L. MRI characteristics of trigeminal nerve involvement in patients with multiple sclerosis. Mult Scler Relat Disord. 2013;2(3):200-3.
[132] Ramina R, Mattei TA, Sória MG, da Silva EB, Jr., Leal AG, Neto MC, et al. Surgical management of trigeminal schwannomas. Neurosurg Focus. 2008;25(6):E6; discussion E.
[133] Borges A, Casselman J. Imaging the trigeminal nerve. Eur J Radiol. 2010;74(2):323-40.
[134] Alberico RA, Fenstermaker RA, Lobel J. Focal enhancement of cranial nerve V after radiosurgery with the Leksell gamma knife: experience in 15 patients with medically refractory trigeminal neuralgia. AJNR Am J Neuroradiol. 2001;22(10):1944-8.